

Continuous-time quantum walks in the presence of a quadratic perturbation

Alessandro Candeloro,¹ Luca Razzoli,² Simone Cavazzoni,² Paolo Bordone,^{2,3} and Matteo G. A. Paris^{1,4}

¹*Quantum Technology Lab, Dipartimento di Fisica Aldo Pontremoli,
Università degli Studi di Milano, I-20133 Milano, Italy*

²*Dipartimento di Scienze Fisiche, Informatiche e Matematiche,
Università di Modena e Reggio Emilia, I-41125 Modena, Italy*

³*Centro S3, CNR-Istituto di Nanoscienze, I-41125 Modena, Italy*

⁴*INFN, Sezione di Milano, I-20133 Milano, Italy*

(Dated: September 3, 2022)

Motivated by their potential use to describe gravity induced perturbations, or next-nearest-neighbor tunnelling, we investigate in details the properties of continuous-time quantum walks (CTQW) with Hamiltonians of the form $\mathcal{H} = L + \lambda L^2$, being L the Laplacian (Kirchoff) matrix of the underlying graph. In particular, we focus attention to CTQW on cycle, complete, and star graphs, as they describe paradigmatic models with low/high connectivity and/or symmetry. At first, we investigate the dynamics of an initially localized walker, looking at the resulting site distribution, mixing, inverse participation ratio, and coherence. We then devote attention to the characterization of perturbation, i.e. the estimation of the perturbation parameter λ using only a snapshot of the walker dynamics. Our analysis shows that a walker on a cycle graph is spreading ballistically independently of the perturbation, whereas on complete and star graphs one observes perturbation-dependent revivals and strong localization phenomena. Concerning characterization, we determine the walker preparations that maximize the Quantum Fisher Information, and assess the performance of position measurement, which turns out to be optimal, or nearly optimal, in several situations of interest. Our study is based on exact analytic derivations supplemented by numerical results, and besides fundamental interest, it may find applications in the design of enhanced algorithms on graphs.

I. INTRODUCTION

Continuous-time quantum walk (CTQW) describes the dynamics of a quantum particle confined to discrete spatial locations, i.e. to the vertices of a graph [1–3]. In this kind of systems, the graph Laplacian L (also referred to as the *Kirchoff* matrix of the graph) plays the role of the free Hamiltonian, i.e. it corresponds to kinetic energy of the particle.

In the present work, we focus attention to quantum walkers propagating on cycle, complete, and star graphs (see Fig. 1), and investigate their dynamics under perturbed Hamiltonians of the form $\mathcal{H} = L + \lambda L^2$. Besides the fundamental interest, there are few reasons to address walkers propagating over these particular graphs, and under the effects of this class of Hamiltonians. The first reason is that the topologies of these graphs describe paradigmatic situations with low (cycle and star) or high (complete) connectivity, as well as low (star) and high (cycle and complete) symmetry.

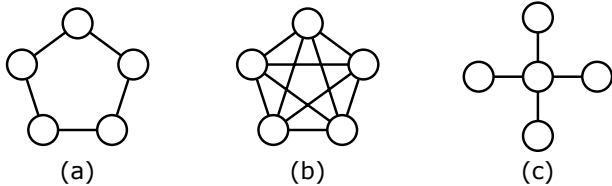


FIG. 1: The three types of graphs considered in the present work: (a) cycle, (b) complete, and (c) star graphs. Examples for $N = 5$ vertices.

At the same time, CTQW Hamiltonians with quadratic perturbation are of interest for at least a couple of reasons. On the one hand, they are suitable to describe gravity corrections to low-energy quantum systems, due to the existence of a minimum measurable length and to the corresponding deformation of the commutation relations [4]. To briefly summarize the point: if we take into account gravity corrections the dynamics of a generic quantum system is governed by the Hamiltonian $\mathcal{H} = \mathcal{H}_0 + \frac{\beta}{m} p_0^4 + \mathcal{O}(\beta^2)$, where $\mathcal{H}_0 = p_0^2/2m + V(\vec{r})$ is the Hamiltonian in the absence of gravity, p_0 is the momentum at low energies, i.e. having the standard representation in position space $p_0 = -i\hbar\nabla$, and $\beta = \ell_{\text{Pl}}^2/2\hbar^2$, where ℓ_{Pl} is the Planck length, is a (small) gravity coupling. This is a quadratic correction in terms of the unperturbed kinetic energy, and more generally in terms of the Laplacian operator. Quadratic corrections of the form λL^2 , on the other hand, represent a physically motivated and convenient way to introduce next-nearest-neighbor hopping in one-dimensional lattices, or intrinsic spin-orbit coupling in two-dimensional ones. Finally, we mention that considering L^2 perturbations is the first step towards the description of dephasing and decoherence processes, which result from making the parameter λ a stochastic process.

Perturbations to ideal CTQW have been investigated earlier[5–12], however with the main focus being about the decoherence effects of stochastic noise, rather than the quantum effects induced by a perturbing Hamiltonian. A notable exception exists, though, given by research about quantum spatial search, where the perturbation induced by the so-called *oracle Hamiltonian* has

been largely investigated as a tool to induce localization on a desired site [13–18]. Here, we analyze the effect of a quadratic perturbation on the dynamics of CTQW, and focus attention to the propagation of an initially localized walker. In order to analyze both semi-classical and genuinely quantum features of the dynamics, we employ a set of different quantifiers, including site distribution, mixing, inverse participation ratio, and coherence. In this framework, we notice that mixing has been studied for CTQWs on some circulant graphs, including the cycle and the complete graph [19], and that two relevant notions of mixing have been introduced: *instantaneous mixing* refers to a situation where there exists a time when the probability distribution of the walker is uniform and *average mixing*, when the probability distribution of the walker is close to uniform in average sense. Mixing has been also employed together with the temporal standard deviation [20] to study the dynamics of CTQW on the cycle graph, whereas a different spectral method has been also introduced to study CTQW on circulant graphs [21, 22]. Coherent transport has been analyzed for CTQW on star graphs [23], showing analytically the occurrence of perfect revivals and strong localization on the initial node.

As a matter of fact, quantum walks have found several applications ranging from universal quantum computation [24] to quantum algorithms [25–29], and to the study of excitation transport on networks [30–32], and biological systems [33, 34]. As such, and due to the diversity of the physical platforms on which quantum walks have been implemented [35, 36], a precise characterization of QW Hamiltonian is desired. In our case, this amounts to determine the value of the coupling parameter λ , quantifying the effects of the quadratic term. In particular, we are going to investigate whether, and to which extent, a snapshot of the walker dynamics at a given time suffices to estimate the value of λ .

The rest of the paper is organized as follows. In Sec. II we address the dynamics of CTQW on different graphs for an initially localized walker. In particular, we study in details the time dependence of the site distribution, the inverse participation ratio, and the coherence. In Sec. III, we focus on the estimation of the parameter of the perturbation by evaluating the Quantum Fisher Information (QFI) as a function of time. We consider initially localized states as well as the states maximizing the QFI. Then, we compare the QFI to the Fisher Information of position measurement for the same states, also determining the simple graphs that allow one to obtain the maximum QFI. In Sec. IV, we summarize and discuss our results and findings. These conclusions are followed by some appendices. In Appendix A we show how the L^2 term in the cycle graph Hamiltonian naturally arises from the spatial discretization of the term in \hat{p}^4 in the continuum Hamiltonian. In Appendix B we provide further details for the analytical results about the dynamics of the CTQWs over different graphs. Eventually, in Appendix C we prove the formulas used throughout

the paper for the (Quantum) Fisher Information, both for the localized states and for the states maximizing the QFI.

II. DYNAMICS

A graph is a pair $G = (V, E)$, where V denotes the non-empty set of vertices and $E \subseteq \{(j, k) | (j, k) \in V^2 \wedge j \neq k\}$ the set of edges. In a graph, the kinetic energy term ($\hbar = 1$) $T = -\nabla^2/2m$ is replaced by $T = \gamma L$, where $\gamma \in \mathbb{R}^+$ is the hopping amplitude of the walk and $L = D - A$ the graph Laplacian, with A the adjacency matrix ($A_{jk} = 1$ if the vertices j and k are connected, 0 otherwise) and D the diagonal degree matrix ($D_{jj} = \deg(j)$). The hopping amplitude γ plays the role of a time-scaling factor, thus the time dependence of the results is significant when expressed in terms of the dimensionless time γt . Please notice that in the following we set $\gamma = \hbar = 1$, and, as a consequence, hereafter time and energy will be dimensionless.

The Hamiltonian we are going to consider is given by

$$\mathcal{H} = \mathcal{H}_0 + \lambda \mathcal{H}_1 = L + \lambda L^2, \quad (1)$$

where the perturbation \mathcal{H}_1 is the square of the unperturbed Hamiltonian $\mathcal{H}_0 = L$ and λ is a dimensionless perturbation parameter. Clearly, \mathcal{H}_0 and \mathcal{H}_1 commute and share a common eigenbasis, in which the total Hamiltonian is diagonal as well. Such eigenbasis is given by the set of the eigenvectors of \mathcal{H}_0 . The exact derivation of Eq. (1) for the cycle graph is shown in Appendix A.

In the following, we provide the matrix and vector representation of operators and states, respectively, in the vertex states basis. We consider finite graphs of order $|V| = N$, where $|\cdot|$ denotes the cardinality, i.e. graphs with N vertices which we index from 0 to $N - 1$. We focus on the dynamics of a walker initially localized in a vertex $j \in V$, i.e. whose initial state is $\rho(t = 0) = |j\rangle\langle j|$.

The time evolution of the system is coherent and ruled by the unitary time-evolution operator

$$\mathcal{U}_\lambda(t) = e^{-i\mathcal{H}t} = \sum_n e^{-i(\varepsilon_n + \lambda \varepsilon_n^2)t} |e_n\rangle\langle e_n|, \quad (2)$$

with \mathcal{H} provided in Eq. (1). The second equality follows from the spectral decomposition of \mathcal{H} , ultimately of L . To study the dynamics of the walker, we address the time dependence of different quantities: the probability distribution over the vertices, the inverse participation ratio, and the coherence.

The (*instantaneous*) probability of finding the walker in the vertex j at time t is given by

$$P(j, t|\lambda) = |\langle j|\mathcal{U}_\lambda(t)|\psi(0)\rangle|^2, \quad (3)$$

whereas the *average* probability of finding it in the vertex j is given by

$$\bar{P}(j|\lambda) = \lim_{T \rightarrow +\infty} \frac{1}{T} \int_0^T P(j, t|\lambda) dt. \quad (4)$$

In addition to the probability distribution of the walker, we also consider the mixing properties for CTQWs on the graph. There are two main notions of *mixing*: *instantaneous mixing* [37] and *average mixing* [38]. Following Refs. [19, 39], we recall the two definitions.

Let $G = (V, E)$ be a graph and let U be the uniform distribution on the vertices of G , i.e. $U(j) = 1/|V|$ for all $j \in V$. Let $P(t|\lambda)$ and $\bar{P}(\lambda)$ be the instantaneous and average probability distributions of a CTQW on G . For $\epsilon \geq 0$

- (i) G has *instantaneous ϵ -uniform mixing* if there exists $t \in \mathbb{R}^+$ such that $\|P(t|\lambda) - U\| \leq \epsilon$. Whenever $\epsilon = 0$ is achievable, G has *instantaneous exactly uniform mixing*.
- (ii) G has *average ϵ -uniform mixing* if $\|\bar{P}(\lambda) - U\| \leq \epsilon$. Whenever $\epsilon = 0$ is achievable, G has the *average uniform mixing* property.

The quantity $\|Q_1 - Q_2\| = \sum_j |Q_1(j) - Q_2(j)|$ is the total variation distance between two probability distributions Q_1 and Q_2 .

The inverse participation ratio (IPR) [8, 40, 41]

$$\mathcal{I}(\rho) = \sum_{j=0}^{N-1} \langle j | \rho(t) | j \rangle^2 = \sum_{j=0}^{N-1} P(j, t | \lambda)^2 \quad (5)$$

allows us to assess the amount of localization in real space of the walker. Indeed, the IPR is bounded from below by $1/N$ (complete delocalization) and from above by 1 (localization on a single vertex). The inverse of $\mathcal{I}(\rho)$ indicates the number of vertices over which the walker is distributed [42]. Hence, the IPR is a particularly useful quantity, since it captures the localization properties of an N -dimensional wave function in a single real value.

A proper measure of quantum coherence is provided by the l_1 norm of coherence [43]

$$\mathcal{C}(\rho) = \sum_{m \neq n} |\rho_{m,n}| = 2 \sum_{m > n} |\rho_{m,n}| = \sum_{m,n} |\rho_{m,n}| - 1, \quad (6)$$

i.e. the sum of the modulus of the off-diagonal elements of the density matrix ρ . The second and the third equalities follow from $\rho^\dagger = \rho$ and $\text{Tr}\{\rho\} = 1$, respectively.

A. Cycle graph

In the cycle graph each vertex is adjacent to 2 other vertices, so its degree is 2. Hence, the Laplacian matrix

$ e_n\rangle$	ε_n	μ_n
$ e_n\rangle = \frac{1}{\sqrt{N}} \sum_{k=0}^{N-1} e^{-i\frac{2\pi n}{N}k} k\rangle$	$2 \left[1 - \cos\left(\frac{2\pi n}{N}\right)\right]$	*
with $n = 0, \dots, N-1$		

TABLE I: Eigenvectors $|e_n\rangle$ and eigenvalues ε_n of the graph Laplacian in the cycle graph. (*) The multiplicity of the eigenvalues depends on the parity of N . In particular, the ground state $n = 0$ is always unique, whereas the highest energy level is unique for even N and doubly degenerate for odd N . Independently of the parity of N , the remaining eigenvalues have multiplicity 2, since $\varepsilon_n = \varepsilon_{N-n}$.

is

$$L = \begin{pmatrix} 2 & -1 & 0 & \cdots & \cdots & 0 & -1 \\ -1 & 2 & -1 & \ddots & & & 0 \\ 0 & -1 & \ddots & \ddots & \ddots & & \vdots \\ \vdots & \ddots & \ddots & \ddots & \ddots & \ddots & \vdots \\ \vdots & & \ddots & \ddots & \ddots & -1 & 0 \\ 0 & & & \ddots & -1 & 2 & -1 \\ -1 & 0 & \cdots & \cdots & 0 & -1 & 2 \end{pmatrix}. \quad (7)$$

This matrix is symmetric and circulant (a special case of Toeplitz matrix). The eigenproblem related to circulant matrices is analytically solved in Ref. [44] and reported in Table I.

The lowest energy level of simple graphs is $\varepsilon = 0$ and admits $(1, \dots, 1)/\sqrt{N}$ as corresponding eigenstate. If the graph is connected, then $\varepsilon = 0$ is not degenerate. Hence, in the cycle graph the ground state ($n = 0$) is unique and is equal to

$$\varepsilon_{min} = 0, \quad (8)$$

$$|e_{min}\rangle = \frac{1}{\sqrt{N}} \sum_{k=0}^{N-1} |k\rangle. \quad (9)$$

Instead, the highest energy level depends on the parity of N and

- (i) is unique for even N ($n = N/2$):

$$\varepsilon_{max} = 4, \quad (10)$$

$$|e_{max}\rangle = \frac{1}{\sqrt{N}} \sum_{k=0}^{N-1} (-1)^k |k\rangle, \quad (11)$$

- (ii) has degeneracy 2 for odd N ($n = (N \pm 1)/2$):

$$\varepsilon_{max} = 2 \left[1 + \cos\left(\frac{\pi}{N}\right)\right], \quad (12)$$

$$|e_{max}\rangle = \frac{1}{\sqrt{N}} \sum_{k=0}^{N-1} (-1)^k e^{\pm i\frac{\pi}{N}k} |k\rangle, \quad (13)$$

where the phase factors are all either with the + sign or with the - sign.

Since for odd N the highest energy level is doubly degenerate, we may be interested in finding the corresponding orthonormal eigenstates having real components [60]. Therefore we define the following states by linearly combining the two eigenstates in Eq. (13) in one case with the plus sign and with the minus sign in the other [61], respectively:

$$|e_{max}^+\rangle = \sqrt{\frac{2}{N}} \sum_{k=0}^{N-1} (-1)^k \cos\left(\frac{\pi}{N}k\right) |k\rangle, \quad (14)$$

$$|e_{max}^-\rangle = \sqrt{\frac{2}{N}} \sum_{k=0}^{N-1} (-1)^k \sin\left(\frac{\pi}{N}k\right) |k\rangle. \quad (15)$$

In a cycle graph all the vertices are equivalent, hence an initially localized state $|j(0)\rangle$ will show the same time evolution independently of the vertex j chosen. According to the spectral decomposition in Table I, we have

$$|j(t)\rangle = \frac{1}{\sqrt{N}} \sum_{n=0}^{N-1} e^{-iE_n^\lambda t} e^{i\frac{2\pi}{N}jn} |e_n\rangle, \quad (16)$$

where $E_n^\lambda := \varepsilon_n + \lambda \varepsilon_n^2$, and $\exp\{i\frac{2\pi}{N}jn\}/\sqrt{N} = \langle e_n | j \rangle$.

The probability of finding the walker in the vertex k at time t for a given value of λ starting from the vertex j is (Fig. 2)

$$\begin{aligned} P_j(k, t|\lambda) &= \frac{1}{N^2} \sum_{n,m=0}^{N-1} e^{-i(E_n^\lambda - E_m^\lambda)t} e^{i\frac{2\pi}{N}(n-m)(j-k)} \quad (17) \\ &= \frac{1}{N} + \frac{2}{N^2} \sum_{\substack{n=0, \\ m>n}}^{N-1} \cos\left[(E_n^\lambda - E_m^\lambda)t - \frac{2\pi}{N}(n-m)(j-k)\right]. \end{aligned} \quad (18)$$

The second equality is simply proved as follows. Let p_{nm} be the summand in the summation in the first line, excluding $1/N^2$. The summation over m can be split in three different summations: one over $m = n$ (providing $\sum_n p_{nn} = N$), one over $m > n$, and one over $m < n$. Since $p_{nm} = p_{mn}^*$, then $\sum_{m<n} p_{nm} = \sum_{m>n} p_{mn}^*$, so $\sum_{m>n} (p_{nm} + p_{mn}^*) = 2 \sum_{m>n} \text{Re}\{p_{nm}\}$, with $\text{Re}\{p_{nm}\} = \cos[\arg(p_{nm})]$. The probability turns out to be symmetric with respect to the starting vertex, i.e. $P_j(j+k, t|\lambda) = P_j(j-k, t|\lambda)$ (see Appendix B1 for the proof).

For the unperturbed system ($\lambda = 0$), the solution of the time-dependent Schrödinger equation for the CTQW on the cycle graph can be expressed in terms of Bessel functions, as pointed out by Ahmadi *et al.* [19]. Inui *et al.* [20] took this hint to study the mixing properties of CTQW on circles. Similarly, Konno [45] studied the CTQW on the line, i.e. the set of integers \mathbb{Z} . Based on Konno's work, Endo *et al.* [46] proved that the spreading of a CTQW on a one-dimensional infinite

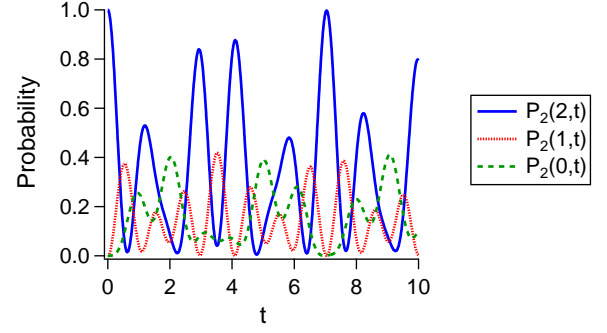


FIG. 2: Probability distribution $P_j(k, t|\lambda)$ of the walker as a function of time in the cycle graph. The walker is initially localized in the vertex $|j=2\rangle$. The probability distribution is symmetric with respect to the central vertex, i.e. $P_j(j+k, t|\lambda) = P_j(j-k, t|\lambda)$. Numerical results suggest that revivals in the starting vertex are most likely not exact. Indeed, to be exact, the periods of the cosine functions entering the definition of the probability (18) have to be commensurable and such periods strongly depend on the choice of N and λ . Results for $N = 5$ and $\lambda = 0.2$.

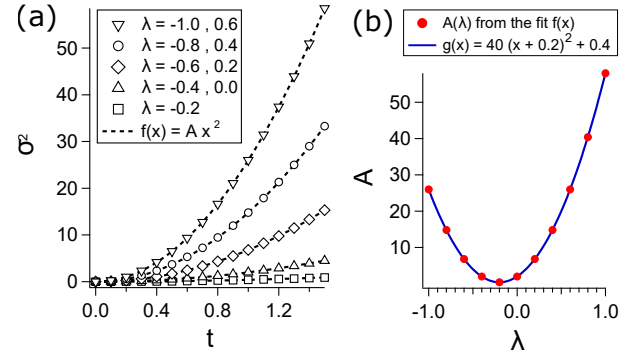


FIG. 3: (a) Variance of the position as a function of time for different values of the parameter λ of the perturbation. The walker is initially localized in the central vertex. Results are symmetric with respect to $\lambda_0 = -1/5$, which is the value for which the nearest-neighbor hopping equals the next-nearest-neighbor one, and for which we observe the lowest variance. Indeed, the latter increases with increasing $|\lambda - \lambda_0|$. (b) The factor A returned by the fit $f(x)$ of the variance grows with λ according to Eq. (20). The spreading is ballistic ($\sigma^2 \propto t^2$) independently of λ .

lattice is ballistic, i.e. the variance of the position is $\sigma^2(t) = \langle \hat{x}(t)^2 \rangle - \langle \hat{x}(t) \rangle^2 \propto t^2$. We expect the same ballistic spreading to characterize the CTQW on a finite cycle as long as the wavefunction does not reach the vertex opposite to the initial one. However, for $\lambda \neq 0$ we can not find a simple expression describing the variance of the position, so we evaluate it numerically. We consider the walker initially localized in the center of the cycle, i.e. $|j(0)\rangle = |N/2 - 1\rangle$ if N is even [62], $|j(0)\rangle = |(N-1)/2\rangle$ if N is odd. We study the time dependence of the variance of the position by fitting the data with the following

function:

$$f(x) = Ax^p. \quad (19)$$

Indeed, the initial value of the variance must be equal to zero, being the walker localized, and for $\lambda = 0$ we must recover the expected ballistic behavior.

Numerically, the power turns out to be $p = 2$ for all the data sets and A to satisfy

$$A(\lambda) = 40(\lambda - \lambda_0)^2 + \frac{2}{5}, \quad (20)$$

with $\lambda_0 = -1/5$ (Fig. 3), so that we expect the variance to be

$$\sigma^2(t) = \left[40(\lambda - \lambda_0)^2 + \frac{2}{5} \right] t^2. \quad (21)$$

The spreading of the walker is ballistic in spite of the perturbation, i.e. for any value of the parameter λ . Increasing $|\lambda - \lambda_0|$ makes the walker spread faster by affecting the prefactor A , not the power of t (see Eq. (19)). Indeed, according to Endo *et al.* [46], the prefactor of t^2 in Eq. (21) is related to the square of the parameter characterizing the speed of the walker. We observe the lowest variance for $\lambda = \lambda_0$, which is the value for which the nearest-neighbor hopping $-(1 + 4\lambda)$ equals the next-nearest-neighbor one λ (see Eq. (A7) in Appendix A). We stress that this relation follows from numerical results, and it holds as long as the walker does not reach the vertex opposite to the initial one (trade-off between the time interval simulated and the number N of vertices). Indeed, we obtained the same results by numerically studying the CTQW on a finite line.

For completeness, we also report in Fig. 4 the numerical results for the probability distribution of Eq. (17) at a given time and at varying λ . We notice that the variance of the position is symmetric with respect to λ_0 (see Eq. (21)) despite the fact that the probability distribution is not.

Upon studying the distance $\|P(t|\lambda) - U\|$ between $P(t|\lambda)$ and the uniform distribution U , we have evidence that instantaneous ϵ -uniform mixing is achievable for $N = 2, 3, 4$, whereas for large N $P(t|\lambda)$ is never close to U , as already conjectured [19]. On the other hand, the average probability follows from Eq. (4) and Eq. (17) (see Appendix B 1 for the details). For even N , the average probability distribution is

$$\bar{P}_j(k|\lambda) = \begin{cases} \frac{2(N-1)}{N^2} & \text{if } k = j \\ \frac{N-2}{N^2} & \text{otherwise.} \end{cases} \quad (22)$$

The total variation distance between the average limiting probability $\bar{P}(\lambda)$ and U is $\|\bar{P}(\lambda) - U\| = 4(N-2)/N^2 \sim 1/N$, so $\bar{P}(\lambda)$ is uniform for $N = 2$, otherwise it ap-

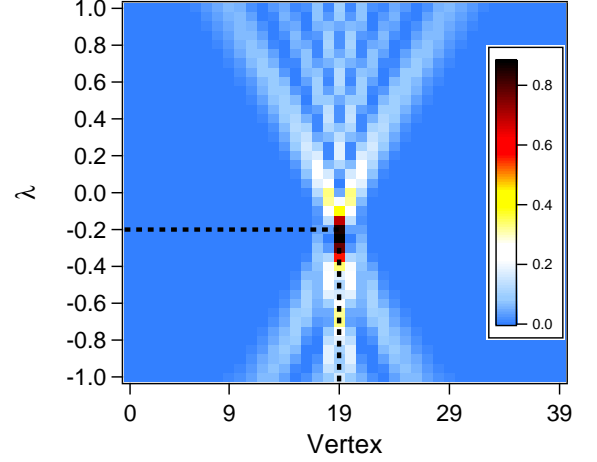


FIG. 4: Map of the probability distribution as a function of the position (vertex) and λ at $t = 1$. The walker is initially localized in the center of the cycle graph ($N = 40$). The vertical dashed line highlights the central vertex, the horizontal one λ_0 , i.e. the value at which the variance of the position is minimum.

proaches U for large N . For odd N , the average probability distribution is

$$\bar{P}_j(k|\lambda) = \begin{cases} \frac{2N-1}{N^2} & \text{if } k = j, \\ \frac{N-1}{N^2} & \text{otherwise.} \end{cases} \quad (23)$$

The total variation distance between the average limiting probability $\bar{P}(\lambda)$ and U is $\|\bar{P}(\lambda) - U\| = 2(N-1)/N^2 \sim 1/N$, so $\bar{P}(\lambda)$ approaches U for large N .

Next, we numerically evaluate the IPR defined in Eq. (5) for the probability distribution in Eq. (17). As expected from the previous results about the probability distribution (see also Fig. 2), the IPR does not show a clear periodicity, it strongly fluctuates, and there are instants of time when it gets closer to 1, meaning that the walker is more localized (Fig. 5). Following the conjecture by Ahmadi *et al.* [19] about the instantaneous uniform mixing, for $N > 4$ also the numerical results about the IPR suggest there is no delocalization. However, for large N the probability distribution in Eq. (17) approaches the uniform one, and so the IPR approaches $1/N$.

Finally, we focus on the time evolution of the coherence of an initially localized walker before it reaches the vertex opposite to the initial one. Under the assumption $t \ll 1$ we can approximate the time evolution of the density matrix as follows:

$$\begin{aligned} \rho(t) &\approx \left(I - i\mathcal{H}t - \frac{1}{2}\mathcal{H}^2t^2 \right) \rho(0) \left(I + i\mathcal{H}t - \frac{1}{2}\mathcal{H}^2t^2 \right) \\ &\approx \rho(0) - it[\mathcal{H}\rho(0) - \rho(0)\mathcal{H}] \\ &\quad - \frac{1}{2}t^2[\mathcal{H}^2\rho(0) - 2\mathcal{H}\rho(0)\mathcal{H} + \rho(0)\mathcal{H}^2]. \end{aligned} \quad (24)$$

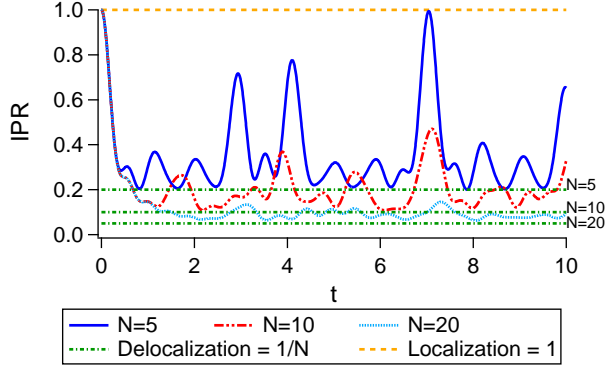


FIG. 5: Inverse participation ratio (IPR) for a walker initially localized in the central vertex of the cycle graph. Numerical results suggest that for $t > 0$ the IPR reaches neither the lower bound $1/N$ (green dashdotted line), i.e. the delocalization, nor the upper bound 1 (orange dashed line), i.e. the localization. The fact that the (de)localization is achievable or not is most likely related to the choice of N and λ . This choice, in turn, might result in the commensurability or incommensurability of the periods of the cosine functions entering the definition of the probability (18). For large N the IPR approaches $1/N$. Indeed, in such a limit the probability distribution of the walker approaches the uniform one (see Eqs. (18)). Results for $\lambda = 0.2$.

Then, we compute the coherence of such approximated state and expand the result up to $\mathcal{O}(t)$. The behavior characterizing the earlier steps of the time evolution of the coherence is therefore

$$\mathcal{C}(\lambda, t) = 4(|\lambda| + |1 + 4\lambda|)t + \mathcal{O}(t^2), \quad (25)$$

which is minimum for $\lambda = -1/4$ (Fig. 6). The latter is the value that makes the nearest-neighbor hopping $-(1 + 4\lambda)$ null and only the next-nearest-neighbor hopping survives (see Eq. (A7) in Appendix A).

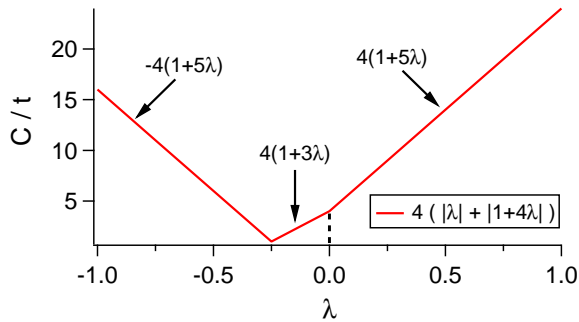


FIG. 6: Ratio of the coherence at short times in Eq. (25) and the time as a function of λ . The minimum is for $\lambda = -0.25$.

The exact numerical results of the coherence at later times are shown in Fig. 7. At short times, we observe that for $\lambda > -1/4$ the coherence increases with $\lambda \rightarrow 1^-$, it is minimum for $\lambda = -1/4$, and for $\lambda < -1/4$ the

n	$ e_n\rangle$	ε_n	μ_n
0	$ e_0\rangle = \frac{1}{\sqrt{N}} \sum_{k=0}^{N-1} k\rangle$	0	1
1	$ e_1^l\rangle = \frac{1}{\sqrt{l(l+1)}} \left(\sum_{k=0}^{l-1} k\rangle - l l\rangle \right)$ with $l = 1, \dots, N-1$	N	$N-1$

TABLE II: Eigenvectors $|e_n\rangle$, eigenvalues ε_n with multiplicity μ_n of the graph Laplacian in the complete graph.

coherence increases with $\lambda \rightarrow -1^+$, as expected from the approximation in Eq. (25).

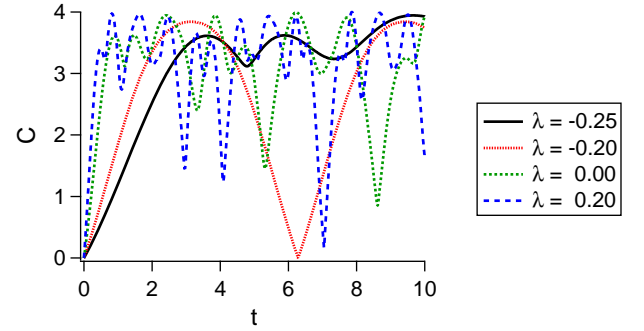


FIG. 7: Coherence for a walker initially localized in the center of the cycle graph with $N=5$. For $t \ll 1$ the minimum is for $\lambda = -0.25$, as expected from the linear approximation in Eq. (25).

B. Complete graph

In the complete graph each vertex is adjacent to all the others, so its degree is $N-1$. Hence, the Laplacian matrix is

$$L = \begin{pmatrix} N-1 & -1 & \cdots & \cdots & -1 \\ -1 & \ddots & \ddots & & \vdots \\ \vdots & \ddots & \ddots & \ddots & \vdots \\ \vdots & & \ddots & \ddots & -1 \\ -1 & \cdots & \cdots & -1 & N-1 \end{pmatrix}. \quad (26)$$

The eigenproblem related to Eq. (26) is solved in Table II. The unperturbed system has two energy levels:

- (i) the level $\varepsilon_0 = 0$, having eigenstate $|e_0\rangle$, is common to all simple graphs and it is not degenerate since the complete graph is connected;
- (ii) the $(N-1)$ -degenerate level $\varepsilon_1 = N$, having orthonormal eigenstates $|e_1^l\rangle$, with $l = 1, \dots, N-1$.

The perturbed Hamiltonian is diagonal in the same eigenbasis, so the unitary evolution in Eq. (2) has matrix representation in the position basis

$$\mathcal{U}_\lambda(t) = \frac{1}{N} \mathbb{J}_N + e^{-i(N+\lambda N^2)t} \left(\mathbb{1}_N - \frac{1}{N} \mathbb{J}_N \right), \quad (27)$$

where \mathbb{J}_N is the $N \times N$ all-ones matrix and $\mathbb{1}_N$ the $N \times N$ identity matrix. In a complete graph all the vertices are equivalent, hence an initially localized state will show the same time evolution $|j(t)\rangle$ independently of the vertex chosen. Indeed, we have

$$\begin{aligned} |j(t)\rangle &= e^{-i(N+\lambda N^2)t} |j\rangle \\ &+ \frac{1}{N} \left(1 - e^{-i(N+\lambda N^2)t} \right) \sum_{i=0}^{N-1} |i\rangle. \end{aligned} \quad (28)$$

To simplify the notation, since all the vertices in the complete graph are equivalent, we denote the starting vertex by $|0\rangle$. The probabilities of finding the walker in $|0\rangle$ or elsewhere, $|1 \leq i \leq N-1\rangle$, at time t for a given value of λ are periodic (Fig. 8)

$$P_0(0, t|\lambda) = 1 - \frac{4(N-1)}{N^2} \sin^2(\omega_N(\lambda)t), \quad (29)$$

$$P_0(i, t|\lambda) = \frac{4}{N^2} \sin^2(\omega_N(\lambda)t), \quad (30)$$

where the angular frequency

$$\omega_N(\lambda) = \frac{1}{2}(N + \lambda N^2) \quad (31)$$

depends on λ . Hence, the walker comes back periodically to the starting vertex and can be found in it with certainty. This occurs for $t_k = 2k\pi/(N + \lambda N^2)$, with $k \in \mathbb{N}$. Increasing the order of the graph makes the angular frequency higher, and $\lim_{N \rightarrow +\infty} P_0(0, t|\lambda) = 1$, while $\lim_{N \rightarrow +\infty} P_0(i, t|\lambda) = 0$. The perturbation affects the periodicity of the probabilities, by increasing or lowering the unperturbed angular frequency in Eq. (31) depending on the choice of N and λ . For $\lambda^* := -1/N \in [-1, 1]$ the angular frequency $\omega_N(\lambda^*) = 0$, so $P_0(0, t|\lambda^*) = 1$ and $P_0(i, t|\lambda^*) = 0$, i.e. the walker remains in the starting vertex all the time. Moreover, the probability distribution is symmetric with respect to λ^* . Indeed, $\omega_N(\lambda^* \pm \lambda) = \pm \lambda N^2/2$ and $\sin^2(\lambda N^2/2) = \sin^2(-\lambda N^2/2)$.

Now, having available the analytical expression of the probability distribution, we consider the mixing. To achieve the instantaneous uniform distribution, we need $P_0(0, t|\lambda) = P_0(i, t|\lambda)$, which leads to $\sin^2(\omega_N(\lambda)t) = N/4$. Hence, the exact instantaneous uniformity is possible only for $N = 2, 3, 4$. The total variation distance between the $P(t|\lambda)$ and the uniform distribution U is $\|P(t|\lambda) - U\| = 2(1 - 1/N)|1 - 4/N \sin^2(\omega_N(\lambda)t)|$. So, for large N $P(t|\lambda)$ is never close to U . On the other hand, the average probabilities are

$$\bar{P}_0(0|\lambda) = 1 - \frac{2(N-1)}{N^2}, \quad (32)$$

$$\bar{P}_0(i|\lambda) = \frac{2}{N^2}. \quad (33)$$

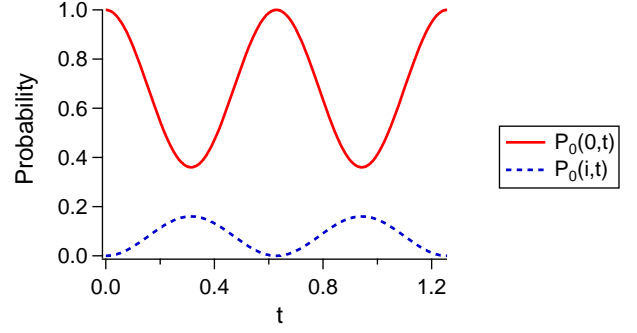


FIG. 8: Probability of finding the walker in the starting vertex $P_0(0, t|\lambda)$ (red solid line) or in any other vertex $P_0(i, t|\lambda)$ (blue dashed line) as a function of time in the complete graph. The walker is initially localized in the vertex $|0\rangle$. Results for $N = 5$ and $\lambda = 0.2$.

The total variation distance between the average limiting probability $\bar{P}(\lambda)$ and U is $\|\bar{P}(\lambda) - U\| = 2(1 - 1/N)(1 - 2/N)$, so $\bar{P}(\lambda)$ is never close to U , except for $N = 2$. In particular, $\lim_{N \rightarrow +\infty} \|\bar{P}(\lambda) - U\| = 2$.

These results about the probability distribution and the mixing are consistent with those by Ahmadi *et al.* [19], who studied the equivalent of our unperturbed system. Indeed, our perturbation only results in a dependence on λ of the period of the probability distribution.

Next, the IPR defined in Eq. (5) for the probability distribution in Eqs. (29)–(30) reads as

$$\begin{aligned} \mathcal{I}(t) &= 1 - \frac{8(N-1)}{N^2} \sin^2(\omega_N(\lambda)t) \\ &+ \frac{16(N-1)}{N^3} \sin^4(\omega_N(\lambda)t). \end{aligned} \quad (34)$$

As expected from the probability distribution, the IPR is periodic (Fig. 9) and it reaches the upper bound 1, i.e. the localization of the walker, for t_k such that $P_0(0, t_k|\lambda) = 1$. Again, the perturbation only affects the periodicity of the IPR. The lower bound $\mathcal{I}_m := \min_t \mathcal{I}$ of the IPR actually depends on N :

$$\mathcal{I}_m = \mathcal{I}(t_l) = \begin{cases} \frac{1}{N} & \text{for } N \leq 4, \\ 1 - \frac{8}{N} + \frac{24}{N^2} - \frac{16}{N^3} & \text{for } N > 4, \end{cases} \quad (35)$$

where

$$t_l \begin{cases} \text{s.t. } \sin^2(\omega_N(\lambda)t_l) = \frac{N}{4} & \text{for } N \leq 4, \\ = \frac{2\pi(1/2 + l)}{N + \lambda N^2} & \text{for } N > 4, \end{cases} \quad (36)$$

with $l \in \mathbb{N}$. Please notice that the two definitions of \mathcal{I}_m match in $N = 4$. For $N \leq 4$ there are instants of time when the walker is delocalized, whereas for $N > 4$ it is never delocalized, since $\mathcal{I}_m > 1/N$. Moreover, $\lim_{N \rightarrow +\infty} \mathcal{I} = 1$, so for large N the walker tends to be localized in the initial vertex.

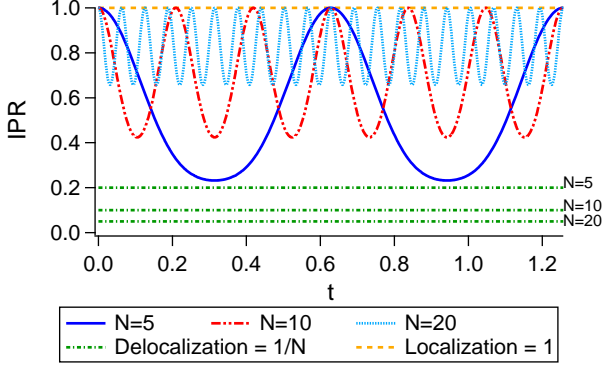


FIG. 9: Inverse participation ratio (IPR) for a walker initially localized in $|0\rangle$ in the complete graph. The IPR periodically reaches the upper bound 1 (orange dashed line), i.e. the localization, but it does not reach the IPR of the delocalized state $1/N$ (green dashdotted line). Indeed, for $N > 4$ the CTQW on the complete graph does not achieve the instantaneous uniform mixing. The lower bound of the IPR is defined in Eq. (35). For $N \rightarrow +\infty$ the IPR approaches 1. Indeed, in such a limit the probability to find the walker in the initial vertex approaches 1, whereas the probability to find it elsewhere approaches 0 (see Eqs. (29)–(30)). Results for $\lambda = 0.2$.

Finally, we focus on the time evolution of the coherence of a walker initially localized in $|0\rangle$. Because of the above mentioned symmetry of the probability distribution, the same symmetry with respect to λ^* affects also the coherence. Indeed, the modulus of the off-diagonal elements of the density matrix can be expressed in terms of the square root of probabilities (see Appendix B). We derive the coherence in Appendix B 2 and the results are shown in Fig. 10. The coherence involves terms like $\sin^2(\omega_N(\lambda)t)$, so it is periodic of period $T = \pi/\omega_N(\lambda)$. The dependence on the perturbation is encoded only in the angular frequency $\omega_n(\lambda)$. As expected, the coherence is minimum for λ^* and for such value it is identically null. For $\lambda \neq \lambda^*$, it periodically reaches the following extrema

$$\max C = \frac{8(N-1)(N-2)}{N^2} \quad \text{for } t_k = \frac{(2k+1)\pi}{N + \lambda N^2}, \quad (37)$$

$$\min C = 0 \quad \text{for } t_k = \frac{2k\pi}{N + \lambda N^2}, \quad (38)$$

with $k \in \mathbb{N}$, and assuming $N \geq 2$.

C. Star graph

In the star graph, the central vertex is adjacent to all the others, so its degree is $N - 1$. On the other hand, the other vertices are only connected to the central one,

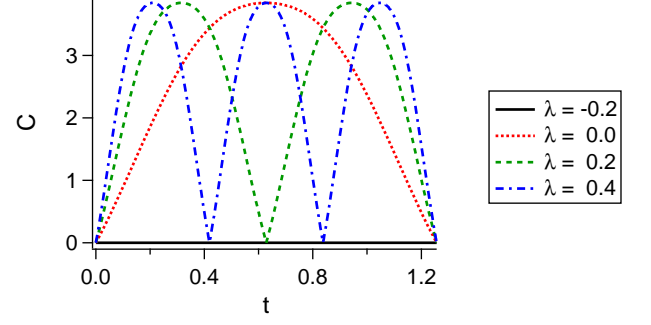


FIG. 10: Coherence for a walker initially localized in $|0\rangle$ in the complete graph with $N = 5$. The coherence is minimum, and in particular it is null, for $\lambda^* = -1/N = -0.2$, as expected. The coherence is symmetric with respect to λ^* , so only data for $\lambda \geq \lambda^*$ are shown.

n	$ e_n\rangle$	ε_n	μ_n
0	$ e_0\rangle = \frac{1}{\sqrt{N}} \sum_{k=0}^{N-1} k\rangle$	0	1
1	$ e_1^l\rangle = \frac{1}{\sqrt{l(l+1)}} \left(\sum_{k=1}^l k\rangle - l l+1\rangle \right)$ with $l = 1, \dots, N-2$	1	$N-2$
2	$ e_2\rangle = \frac{1}{\sqrt{N(N-1)}} \left[(N-1) 0\rangle - \sum_{k=1}^{N-1} k\rangle \right]$	N	1

TABLE III: Eigenvectors $|e_n\rangle$, eigenvalues ε_n with multiplicity μ_n of the graph Laplacian in the star graph.

thus their degree is 1. Hence, the Laplacian matrix is

$$L = \begin{pmatrix} N-1 & -1 & \cdots & \cdots & -1 \\ -1 & 1 & 0 & \cdots & 0 \\ \vdots & 0 & \ddots & \ddots & \vdots \\ \vdots & \vdots & \ddots & \ddots & 0 \\ -1 & 0 & \cdots & 0 & 1 \end{pmatrix}, \quad (39)$$

where the first row and column refer to the central vertex, which we label with the 0-th index.

The eigenproblem related to Eq. (39) is solved in Table III. The unperturbed system has three energy levels:

- (i) the level $\varepsilon_0 = 0$, having eigenstate $|e_0\rangle$, is common to all simple graphs and it is not degenerate since the star graph is connected;
- (ii) the $(N-2)$ -degenerate level $\varepsilon_1 = 1$, having orthonormal eigenstates $|e_1^l\rangle$, with $l = 1, \dots, N-2$;
- (iii) the level $\varepsilon_1 = N$, having eigenstate $|e_2\rangle$.

Again, the perturbed Hamiltonian is diagonal in the same eigenbasis, so the unitary evolution in Eq. (2) has

matrix representation

$$\mathcal{U}_\lambda(t) = \frac{1}{N} \mathbb{J}_N + e^{-i(1+\lambda)t} \mathbb{Y}_N + e^{-i(N+\lambda N^2)t} \mathbb{W}_N, \quad (40)$$

where

$$\mathbb{Y}_N = \left(\begin{array}{c|ccc} 0 & 0 & \cdots & 0 \\ \hline 0 & & & \\ \vdots & & & \\ 0 & & & \end{array} \begin{array}{c} \mathbb{1}_{N-1} - \frac{1}{N-1} \mathbb{J}_{N-1} \\ \\ \\ \end{array} \right) \quad (41)$$

and

$$\mathbb{W}_N = \left(\begin{array}{c|ccc} 1 - \frac{1}{N} & -\frac{1}{N} & \cdots & -\frac{1}{N} \\ \hline -\frac{1}{N} & & & \\ \vdots & & & \\ -\frac{1}{N} & & & \end{array} \begin{array}{c} \\ \frac{1}{N(N-1)} \mathbb{J}_{N-1} \\ \\ \end{array} \right). \quad (42)$$

For an initially localized state, there are two different time evolutions. If at $t = 0$ the walker is in the central vertex $|0\rangle$, then the time evolution is equal to the corresponding one in the complete graph of the same size (see Eq. (28) for $j = 0$). Therefore, also the resulting probability distribution and the coherence are equal between star and complete graph. Instead, if at $t = 0$ the walker is localized in any of the outer vertices, then we have a different time evolution, e.g.

$$\begin{aligned} |1(t)\rangle &= \frac{1}{N} \sum_{i=0}^{N-1} |i\rangle + e^{-i(1+\lambda)t} \left(|1\rangle - \frac{1}{N-1} \sum_{i=1}^{N-1} |i\rangle \right) \\ &+ e^{-i(N+\lambda N^2)t} \left(-\frac{1}{N} |0\rangle + \frac{1}{N(N-1)} \sum_{i=1}^{N-1} |i\rangle \right). \end{aligned} \quad (43)$$

Please notice that the difference among the vertices in the star graph is only between the central vertex $|0\rangle$ and the outer ones $|1 \leq i \leq N-1\rangle$. All the outer vertices are equivalent, and this is the reason why we can focus on $|1\rangle$. Indeed, keeping the central vertex as $|0\rangle$, we can always relabel the outer vertices in such a way that the starting vertex is denoted by $|1\rangle$.

The probabilities of finding the walker in the central vertex $|0\rangle$, in the starting vertex $|1\rangle$ or in any other outer vertex $|2 \leq i \leq N-1\rangle$ at time t for a given value of λ

are respectively (Fig. 11)

$$P_1(0, t|\lambda) = \frac{4}{N^2} \sin^2(\omega_N(\lambda)t), \quad (44)$$

$$\begin{aligned} P_1(1, t|\lambda) &= 1 - \frac{4}{N(N-1)} \left[(N-2) \sin^2(\omega_1(\lambda)t) \right. \\ &\quad + \frac{N-2}{N-1} \sin^2[(\omega_N(\lambda) - \omega_1(\lambda))t] \\ &\quad \left. + \frac{1}{N} \sin^2(\omega_N(\lambda)t) \right], \end{aligned} \quad (45)$$

$$\begin{aligned} P_1(i, t|\lambda) &= \frac{4}{N(N-1)} \left[\sin^2(\omega_1(\lambda)t) \right. \\ &\quad + \frac{1}{N-1} \sin^2[(\omega_N(\lambda) - \omega_1(\lambda))t] \\ &\quad \left. - \frac{1}{N} \sin^2(\omega_N(\lambda)t) \right], \end{aligned} \quad (46)$$

where the angular frequency is defined in Eq. (31). In particular, $P_1(0, t|\lambda)$ is periodic with period $T_N := \pi/\omega_N(\lambda)$, it is symmetric with respect to $\lambda^* = -1/N$, and $P_1(0, t|\lambda^*) = 0$, which means that the walker lives only in the outer vertices of the star graph. Instead, $P_1(1, t|\lambda)$ and $P_1(i, t|\lambda)$ are periodic if and only if the periods T_1 , T_N , and $\pi/(\omega_N(\lambda) - \omega_1(\lambda))$ of the summands are commensurable [47] (we address the periodicity of the probability distribution in Appendix B3). When this happens, then the overall probability distribution is periodic. This happens also for the values $\lambda = -1, -1/N, -1/(N+1)$, which make null ω_1 , ω_N , and $\omega_N - \omega_1$, respectively. For $P_1(1, t|\lambda)$ and $P_1(i, t|\lambda)$ we can not find a symmetry with respect to λ . Increasing the order of the graph makes the angular frequency higher, and $\lim_{N \rightarrow +\infty} P_1(1, t|\lambda) = 1$, while $\lim_{N \rightarrow +\infty} P_1(0, t|\lambda) = \lim_{N \rightarrow +\infty} P_1(i, t|\lambda) = 0$. Again, the perturbation affects the probabilities only through the angular frequency $\omega_N(\lambda)$.

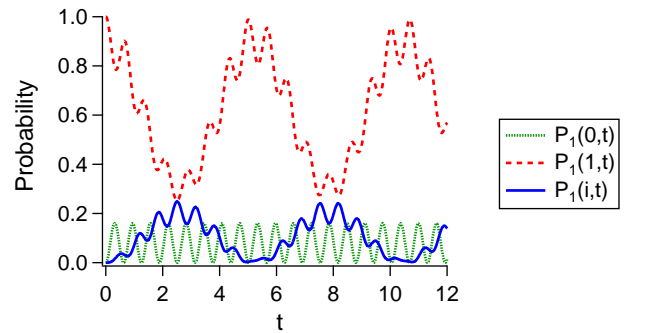


FIG. 11: Probability of finding the walker in the central vertex $P_1(0, t|\lambda)$ (green dotted line), in the starting vertex $P_1(1, t|\lambda)$ (red dashed line) or in any other vertex $P_1(i, t|\lambda)$ (blue solid line) as a function of time in the star graph. The walker is initially localized in the vertex $|1\rangle$. Results for $N = 5$ and $\lambda = 0.2$.

To study the instantaneous exactly uniform mixing we assess $\|P(t|\lambda) - U\|$ together with the IPR. By considering $P_1(0, t|\lambda) = 1/N$ we notice that, independently of λ ,

the instantaneous exactly uniform mixing is never achievable for $N > 4$, so $P(t|\lambda)$ is never close to U for large N . Instead, for $2 \leq N \leq 4$ the mixing properties strongly depend on the choice of the couple (N, λ) . The instantaneous exactly uniform mixing is never achievable for λ^* , since $P_1(0, t|\lambda^*) = 0 \forall t$, whereas it is achievable, e.g., for $2 \leq N \leq 4 \wedge \lambda = -1/(N+1)$ and for $N = 2 \wedge \lambda = -1$. On the other hand, the average probabilities are

$$\bar{P}_1(0|\lambda) = \frac{2}{N^2}, \quad (47)$$

$$\bar{P}_1(1|\lambda) = \frac{2 + N(N-1)^2(N-2)}{N^2(N-1)^2}, \quad (48)$$

$$\bar{P}_1(i|\lambda) = \frac{2[1 + N(N-1)]}{N^2(N-1)^2}. \quad (49)$$

Also in this case, $\bar{P}(\lambda)$ is never close to U , except for $N = 2$. In particular, $\lim_{N \rightarrow +\infty} \|\bar{P}(\lambda) - U\| = 2$. Next, we numerically evaluate the IPR defined in Eq. (5) for the probability distribution in Eqs. (44)–(46) according to

$$\mathcal{I}(t) = P_1^2(0, t|\lambda) + P_1^2(1, t|\lambda) + (N-2)P_1^2(i, t|\lambda). \quad (50)$$

As already pointed out before for the probability distribution, the periodicity of the IPR relies upon the commensurability of the periods of the summands. However, from Fig. 12 we observe that the IPR oscillates between 1 and its minimum value, which grows with N , similarly to what happens in the complete graph. Even in this case, for $N \rightarrow +\infty$ the IPR approaches 1, since the probability to find the walker in the initial vertex approaches 1, whereas the probability to find it elsewhere approaches 0. According to the previous remarks about the instantaneous exactly uniform mixing, for $N > 4$ the IPR is never close to $1/N$, i.e. the walker is never uniformly delocalized. On the other hand, when the probability distribution is periodic (for λ in Eq. (B32)), the IPR periodically reaches 1, since the walker is initially localized in a vertex and so it periodically comes back to it.

Let us now focus on the time evolution of the coherence of a walker initially localized in $|1\rangle$. Unlike the case of the complete graph, in the star graphs we do not expect the coherence to be symmetric with respect to λ . We derive the coherence in Appendix B 3 and the results are shown in Fig. 13. The coherence shows a complex structure of local maxima and minima. However, the coherence is smoother and periodic for the values of λ defined in Eq. (B32) in Appendix B 3, e.g. $\lambda = -1, -1/N, -1/(N+1)$. Indeed, for such values the overall probability distribution (44)–(46) is periodic.

III. CHARACTERIZATION

In this section we address the estimation of the parameter λ that quantifies the amplitude of the perturbation \mathcal{H}_1 in the CTQW Hamiltonian (1). Our main goal is to

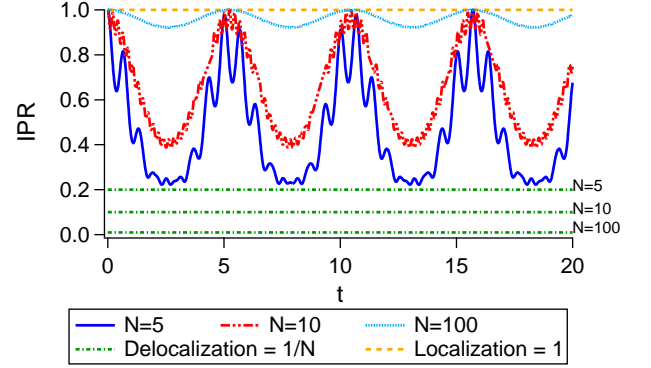


FIG. 12: Inverse participation ratio (IPR) for a walker initially localized in $|1\rangle$ in the star graph. The lower bound $1/N$ (delocalization) is represented by the green dashdotted line, whereas the upper bound 1 (localization) by the orange dashed line. For $N \rightarrow +\infty$ the IPR approaches 1. Indeed, in such a limit the probability to find the walker in the initial vertex approaches 1, whereas the probability to find it elsewhere approaches 0 (see Eqs. (44)–(46)). Results for $\lambda = 0.2$.

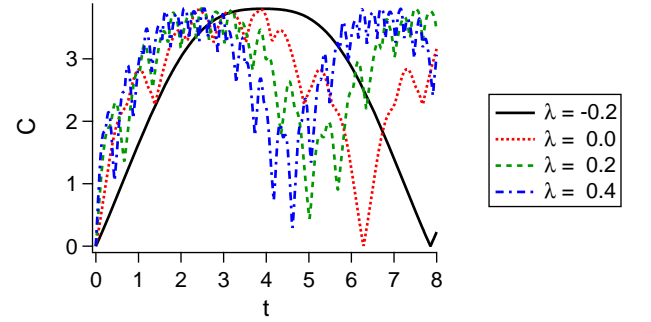


FIG. 13: Coherence for a walker initially localized in $|1\rangle$ in the star graph with $N = 5$. The coherence is smooth and periodic for $\lambda^* = -1/N = -0.2$.

assess whether, and to which extent, we may determine the value of λ using only a snapshot of the walker dynamics, i.e. performing measurements at a given time t . To this aim, let us briefly review some useful concepts from classical and quantum estimation theory [48]. The main goal of classical estimation theory is to find an *estimator*, i.e a function $\hat{\lambda}$ that, taking as input n experimental data $\{x_i\}_{i=1, \dots, n}$ whose probabilistic distribution $P(x_i|\lambda)$ depends on λ , gives the most precise estimate of the parameter. A particular class of $\hat{\lambda}$ are the *unbiased estimators*, for which the expectation value is the actual value of the parameter λ , i.e.

$$E_\lambda[\hat{\lambda}] = \int dx P(x|\lambda) \hat{\lambda}(x) \equiv \lambda. \quad (51)$$

The main result regarding the precision of an estimator $\hat{\lambda}$ is given by the Cramér-Rao Bound, which sets a lower bound on the variance of any unbiased estimator $\hat{\lambda}$, provided that the family of distribution $P(x|\lambda)$ realizes

a so-called *regular statistical model* (see below). In this case, the variance of any unbiased estimator $\hat{\lambda}$ satisfies the inequality

$$\sigma^2(\hat{\lambda}) \geq \frac{1}{n\mathcal{F}_c(\lambda)}, \quad (52)$$

where $\mathcal{F}_c(\lambda)$ is the Fisher Information (FI) of the probability distribution $P(x|\lambda)$

$$\mathcal{F}_c(\lambda) = \int dx \frac{\partial_\lambda(P(x|\lambda))^2}{P(x|\lambda)}. \quad (53)$$

We remind that regular models are those with a constant support, i.e. the region for which $P(x|\lambda) \neq 0$ does not depend on the parameter λ , and with non-singular Fisher information. If the hypotheses above are not satisfied, estimators with vanishing variance may be easily found. Optimal estimators are those saturating the above inequality, and it can be proved that for $n \rightarrow +\infty$ maximum likelihood estimators attain the lower bound [49].

In a quantum scenario, the parameter must be encoded in the density matrix of the system. In turn, a *quantum statistical model* is defined as a family of quantum states $\{\rho_\lambda\}$ parametrized by the value of λ . In order to extract information from the system, we need to perform measurements, i.e. positive operator-valued measure (POVM) $\{\mathcal{E}_m\}$, where m is a continuous or discrete index labeling the outcomes. Thanks to the Born rule, a conditional distribution naturally arises

$$P(m|\lambda) = \text{Tr}\{\rho_\lambda \mathcal{E}_m\}. \quad (54)$$

Unlike the classical regime, the probability depends both on the state and on the measurement, so we can suitably choose them to get better estimates. In particular, given a family of quantum states $\{\rho_\lambda\}$, we can find a POVM which maximizes the FI $\mathcal{F}_c(\lambda)$, i.e.

$$\mathcal{F}_c(\lambda) \leq \mathcal{F}_q(\lambda) = \text{Tr}\{\rho_\lambda \Lambda_\lambda^2\}, \quad (55)$$

where Λ_λ is the Symmetric Logarithmic Derivative (SLD) implicitly defined as

$$\frac{\rho_\lambda \Lambda_\lambda + \Lambda_\lambda \rho_\lambda}{2} = \partial_\lambda \rho_\lambda, \quad (56)$$

and $\mathcal{F}_q(\lambda)$ is the Quantum Fisher Information (QFI). The optimal POVM saturating the inequality in Eq. (55) is given by the projectors on the eigenspaces of the SLD. Since $\mathcal{F}_q(\lambda) = \max_{\mathcal{E}_m} \{\mathcal{F}_c(\lambda)\}$, we have a more precise bound on $\sigma^2(\hat{\lambda})$ which goes by the name of Quantum Cramér-Rao (QCR) inequality

$$\sigma^2(\hat{\lambda}) \geq \frac{1}{n\mathcal{F}_q(\lambda)}. \quad (57)$$

This establishes the ultimate lower bound of the precision in estimating a parameter λ encoded in a quantum state. Notice that the QCR is valid for *regular quantum*

statistical model, i.e. families of quantum states made of density matrices with constant rank (i.e. the rank does not depend on the parameter) and leading to a nonsingular QFI [50–52].

In the present work we focus on pure states subjected to the unitary evolution in Eq. (2), i.e. $|\psi_\lambda(t)\rangle = \mathcal{U}_\lambda(t) |\psi(0)\rangle$. For such states the QFI reads as

$$\mathcal{F}_q(t, \lambda) = 4 \left[\langle \partial_\lambda \psi_\lambda(t) | \partial_\lambda \psi_\lambda(t) \rangle - |\langle \psi_\lambda(t) | \partial_\lambda \psi_\lambda(t) \rangle|^2 \right]. \quad (58)$$

Dealing with CTQWs on a graph, a reasonable and significant measurement is the position one. For such a measurement the FI reads as

$$\mathcal{F}_c(t, \lambda) = \sum_{i=0}^{N-1} \frac{(\partial_\lambda P(i, t|\lambda))^2}{P(i, t|\lambda)}, \quad (59)$$

where $P(i, t|\lambda)$ is the conditional probability of finding the walker in the i -th vertex at time t when the value of the parameter is λ .

For a unitary time evolution where the perturbation \mathcal{H}_1 commutes with the unperturbed Hamiltonian \mathcal{H}_0 (which is our case, see Eq. (1)), the evolution simplifies to

$$\mathcal{U}_\lambda(t) = e^{-it(\mathcal{H}_0 + \lambda \mathcal{H}_1)} = e^{-it\mathcal{H}_0} e^{-it\lambda \mathcal{H}_1}. \quad (60)$$

Then, the QFI has a simple representation in terms of the perturbation and of time. Indeed, if our probe $|\psi\rangle$ at time $t = 0$ does not depend on λ and undergoes the evolution $\mathcal{U}_\lambda(t)$, at a later time $t > 0$ we have that

$$|\psi_\lambda(t)\rangle = e^{-it\mathcal{H}_0} e^{-it\lambda \mathcal{H}_1} |\psi\rangle, \quad (61)$$

$$|\partial_\lambda \psi_\lambda(t)\rangle = e^{-it\mathcal{H}_0} (-it\mathcal{H}_1) e^{-it\lambda \mathcal{H}_1} |\psi\rangle. \quad (62)$$

Thus, since $[\mathcal{H}_0, \mathcal{H}_1] = 0$, we can write the QFI as a function of the initial probe and time as follows

$$\begin{aligned} \mathcal{F}_q(t) &= 4t^2 [\langle \psi | \mathcal{H}_1^2 | \psi \rangle - \langle \psi | \mathcal{H}_1 | \psi \rangle^2] \\ &= 4t^2 \langle (\Delta \mathcal{H}_1)^2 \rangle. \end{aligned} \quad (63)$$

The QFI is therefore quadratic in time and the quantity in square brackets can be interpreted as the variance of the operator \mathcal{H}_1 on the probe $|\psi\rangle$. We emphasize that the QFI does not depend on the parameter λ to be estimated. This is due to the unitary nature of the interaction, and to the fact that the probe $|\psi\rangle$ does not initially depend on λ . Please refer to Appendix C for the details about the analytical derivation of the formulas of the QFI and FI shown in the following.

A. Localized states

The first probes we use to study the achievable precision on the estimation of λ are the localized state $|\psi(0)\rangle = |j\rangle$, for which we have already found the dynamics in the previous section. In the following we denote the state obtained under the unitary time evolution by $|j(t, \lambda)\rangle$.

1. Cycle graph

The time evolution of an initially localized state in the complete graph is provided in Eq. (16). For this state, the QFI turns out to be

$$\mathcal{F}_q(t) = 136t^2. \quad (64)$$

We point out that the QFI is independent of N , of the parameter λ , and it is quadratic in time (consistently with Eq. (63)). Because of the cumbersome expression of the probability distribution in Eq. (18), we numerically evaluate the FI by definition (see Eq. (59)) and we just plot the results in Fig. 14. Numerical results suggest that the FI never reaches the QFI. However, due to the form of the probability distribution (18), particular behaviors strongly depend on the choice of N and λ .

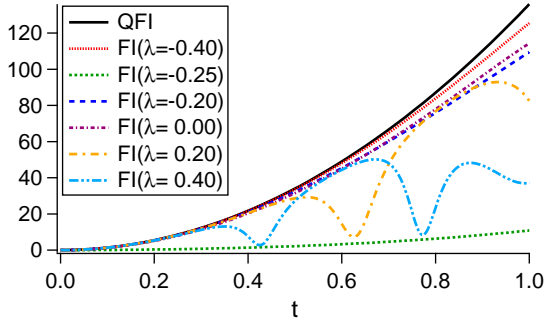


FIG. 14: Quantum (black solid line) and classical Fisher Information (colored non-solid lines) of position measurement for an initially localized state in the cycle graph. Results for $N = 5$.

2. Complete Graph

The time evolution of an initially localized state in the complete graph is provided in Eq. (28). For this state, the QFI turns out to be

$$\mathcal{F}_q(N, t) = 4N^2(N-1)t^2. \quad (65)$$

We point out that the QFI is $\mathcal{O}(N^3)$, is independent of the parameter λ , and it is quadratic in time (consistently with Eq. (63)).

The FI of position measurement is

$$\mathcal{F}_c(N, t, \lambda) = \frac{4N^4 t^2 (N-1) \cos^2(\omega_N(\lambda)t)}{N^2 - 4(N-1) \sin^2(\omega_N(\lambda)t)}, \quad (66)$$

with $\omega_N(\lambda)$ defined in Eq. (31). As expected according to the symmetry of the graph, both the QFI and the FI do not depend on the starting vertex j , i.e. the estimation is completely indifferent to the choice of the initially localized state. Instead, unlike the QFI, the FI does depend on λ . As observed for the probability distribution and the coherence in Sec. II B, even the FI

is symmetric with respect to $\lambda^* = -1/N$. In particular, $\mathcal{F}_c(t, \lambda^*) = \mathcal{F}_q(t)$. However, we recall that $P_0(0, t|\lambda^*) = 1$ and $P_0(i, t|\lambda^*) = 0$, i.e. the walker is in the starting vertex all the time. In this case the hypotheses leading to the Cramér-Rao Bound (52) do not hold, since the model is not regular, and the bound may be easily surpassed. Indeed, if we perform the measurement described by the POVM $\{|0\rangle\langle 0|, \mathbb{1} - |0\rangle\langle 0|\}$, the variance of the estimator is identically zero, outperforming both classical and quantum bounds.

For $\lambda \neq \lambda^*$, the periodicity of the probabilities in Eqs. (29)–(30) results in a dependence of the FI on λ and an analogous oscillating behavior (Fig. 15). The FI reaches periodically its local maxima when the numerator is maximum and the denominator is minimum, and these maxima saturate the Quantum Cramér-Rao Bound

$$\mathcal{F}_c(t_k, \lambda) = \mathcal{F}_q(t_k, \lambda). \quad (67)$$

This occurs for $t_k = 2k\pi/(N + \lambda N^2)$, with $k \in \mathbb{N}$, i.e. when the walker is completely localized and we definitely find it in the initial vertex (see Eq. (29)). Indeed, in the probability distribution the parameter λ is encoded only in the angular frequency, thus knowing when the walker is certainly in the initial vertex means knowing exactly its period, and thus the parameter λ . However, to perform such a measurement one needs some *a priori* knowledge of the value of the parameter. In fact, the POVM saturating the Quantum Cramér-Rao Bound (57) strongly depends on the parameter λ .

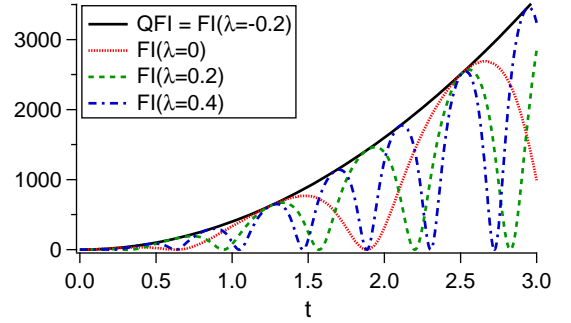


FIG. 15: Quantum (black solid line) and classical Fisher Information (colored non-solid lines) of position measurement for an initially localized state in the complete graph. The same results are obtained for a walker initially localized in the central vertex $|0\rangle$ of the star graph of the same size. The FI is optimal for $\lambda^* = -1/N = -0.2$. Results for $N = 5$.

3. Star Graph

The time evolution of the state localized in the center of the star graph is equivalent to that of a localized state in the complete graph, as already pointed out in Sec. II C. Then, for this state the QFI and FI are provided in Eq. (65) and in Eq. (66), respectively (see Fig. 15).

Things change when we consider a walker initially localized in one of the outer vertices of the star graph, i.e. in any vertex of index $1 \leq j \leq N-1$. Its time evolution is provided in Eq. (43) and the corresponding QFI turns out to be

$$\mathcal{F}_q(N, t) = 4t^2(N^2 + N - 2). \quad (68)$$

We point out that the QFI is $\mathcal{O}(N^2)$, is independent of the parameter λ , and it is quadratic in time (consistently with Eq. (63)).

Because of the cumbersome expression of the FI (see Appendix C 4), here we just plot the results in Fig. 16. Unlike the complete graph, for the star graph there is no saturation of the Quantum Cramér-Rao Bound. Notice, however, that for $\lambda^* = -1/N$ the walker cannot reach the central site and, in principle, one may exploit this feature to build a non regular model, as we discussed in the previous Section.

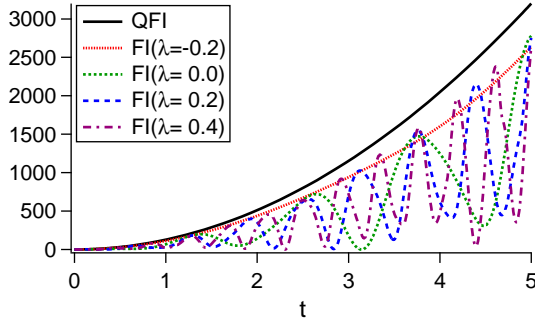


FIG. 16: Quantum (black solid line) and classical Fisher Information (colored non-solid lines) of position measurement for a walker initially localized in an outer vertex of the star graph. Results for $N = 5$.

B. States maximizing the QFI

In the previous Sections, we have studied how localized states behave as quantum probes for estimating the parameter λ of the perturbation. However, we might be interested in finding the best estimate for such parameter by searching for the state ρ_λ maximizing the QFI, hence minimizing the variance $\sigma^2(\hat{\lambda})$. For this purpose, it is worth introducing an alternative formula for QFI. When there is only one parameter to be estimated and the state is pure, the QFI reads as

$$\mathcal{F}_q(\lambda, t) = \lim_{\delta\lambda \rightarrow 0} \frac{8(1 - |\langle \psi_\lambda(t) | \psi_{\lambda+\delta\lambda}(t) \rangle|)}{\delta\lambda^2}, \quad (69)$$

where $|\psi_\lambda(t)\rangle = \exp\{-i\mathcal{H}t\}|\psi_\lambda(0)\rangle$. Eq. (69) involves the modulus of the following scalar product:

$$\langle \psi_\lambda(t) | \psi_{\lambda+\delta\lambda}(t) \rangle = \langle \psi(0) | U_{\delta\lambda}(t) | \psi(0) \rangle, \quad (70)$$

where

$$\begin{aligned} U_{\delta\lambda}(t) &:= e^{+i(\mathcal{H}_0 + \lambda\mathcal{H}_1)t} e^{-i[\mathcal{H}_0 + (\lambda + \delta\lambda)\mathcal{H}_1]t} \\ &= e^{-i\delta\lambda\mathcal{H}_1 t}, \end{aligned} \quad (71)$$

is a unitary operator given by the product of two unitary operators related to the time evolutions for λ and $\lambda + \delta\lambda$. The last equality holds since $[\mathcal{H}_0, \mathcal{H}_1] = 0$.

The QFI strongly depends on the quantum state considered. To maximize the QFI, we recall the following lemma by K. R. Parthasarathy [53].

Lemma 1. *Let W be any unitary operator in the finite dimensional complex Hilbert space \mathcal{H} with spectral resolution $\sum_{j=1}^k e^{i\theta_j} P_j$ where $e^{i\theta_1}, \dots, e^{i\theta_k}$ are the distinct eigenvalues of W with respective eigenprojections P_1, \dots, P_k . Define*

$$m(W) = \min_{\|\psi\|=1} |\langle \psi | W \psi \rangle|^2. \quad (72)$$

Then the following hold:

- (i) *If there exists a unit vector $|\psi_0\rangle$ such that $\langle \psi_0 | W \psi_0 \rangle = 0$, then $m(W) = 0$.*
- (ii) *If $\langle \psi | W \psi \rangle > 0$ for every unit vector $|\psi\rangle$, then*

$$m(W) = \min_{i \neq j} \cos^2 \left(\frac{\theta_i - \theta_j}{2} \right). \quad (73)$$

Furthermore, when the right-hand side is equal to $\cos^2 \left(\frac{\theta_{i_0} - \theta_{j_0}}{2} \right)$,

$$m(W) = |\langle \psi_0 | W \psi_0 \rangle|^2 \quad (74)$$

where

$$|\psi_0\rangle = \frac{1}{\sqrt{2}}(|e_{i_0}\rangle + |e_{j_0}\rangle) \quad (75)$$

and $|e_{i_0}\rangle$ and $|e_{j_0}\rangle$ are arbitrary unit vectors in the range of P_{i_0} and P_{j_0} respectively.

The idea is to exploit the Lemma to compute the QFI, by letting $|\psi(0)\rangle = |\psi_0\rangle$ and by identifying W with $U_{\delta\lambda}(t)$, since $\langle \psi_\lambda(t) | \psi_{\lambda+\delta\lambda}(t) \rangle = \langle \psi_0 | U_{\delta\lambda}(t) | \psi_0 \rangle$, so that

$$\mathcal{F}_q(\lambda, t) = \lim_{\delta\lambda \rightarrow 0} \frac{8 \left[1 - \sqrt{m(U_{\delta\lambda}(t))} \right]}{\delta\lambda^2}. \quad (76)$$

Indeed, the state $|\psi_0\rangle$ in Eq. (75) maximizes the QFI by minimizing the modulus of the scalar product in Eq. (70). The unit vectors involved by $|\psi_0\rangle$ are eigenvectors of the unitary operator in Eq. (71) and so, ultimately, of \mathcal{H}_1 . In particular, such states are those whose eigenvalues minimize Eq. (73). The eigenvalues of the unitary operator in Eq. (71) are $e^{i\theta_j} = e^{-i\delta\lambda t \varepsilon_j^2}$, with $\{\varepsilon_j^2\}$ eigenvalues of $\mathcal{H}_1 = \mathcal{H}_0^2$, being $\{\varepsilon_j\}$ those of $\mathcal{H}_0 = L$. Thus, we can identify $\theta_j = -\delta\lambda t \varepsilon_j^2$. Because of this relation,

and being $t \geq 0$, we may assume $|e_{i_0}\rangle$ and $|e_{j_0}\rangle$ to be the eigenstates corresponding to the lowest and the highest energy eigenvalue. Indeed, in the limit for $\delta\lambda t \rightarrow 0$ the cosine in Eq. (73) is minimized by maximizing the difference $\theta_i - \theta_j$. Then, the QFI reads as follows:

$$\mathcal{F}_q(t) = t^2(\varepsilon_{max}^2 - \varepsilon_{min}^2)^2 = t^4 \varepsilon_{max}^4. \quad (77)$$

Because of the choice of the state $|\psi_0\rangle$, which involves the lowest and the highest energy eigenstates, the first equality follows from Eq. (63), whereas the second equality holds since $\varepsilon_{min} = 0$ for simple graphs. We obtain the same result by taking the limit for $\delta\lambda t \rightarrow 0$ of Eq. (73), as shown in Appendix C 1. An eventual phase difference between the two eigenstates in Eq. (75) would result in the same QFI, but a different FI, as shown in Appendix C 5.

1. Cycle graph

The cycle graph is sensitive to the parity of N . At $t = 0$ the state $|\psi_0\rangle$ maximizing the QFI is:

$$|\psi_0^{(\pm)}\rangle = \frac{1}{\sqrt{2}}(|e_{min}\rangle + |e_{max}^{(\pm)}\rangle), \quad (78)$$

where $|e_{min}\rangle$ is the ground state, corresponding to the eigenvalue $\varepsilon_{min} = 0$, while $|e_{max}^{(\pm)}\rangle$ is the eigenstate corresponding to the highest energy level and it depends on the parity of N . For even N it is unique, whereas for odd N the highest energy level is doubly degenerate, which is the reason for the \pm sign (see Eqs. (14)–(15) and Table I). In particular, for even N the optimal state reads as

$$|\psi_0\rangle = \sqrt{\frac{2}{N}} \sum_{k=0}^{N/2-1} |2k\rangle, \quad (79)$$

i.e. a superposition of the position states corresponding to even vertices.

The resulting QFI is

$$\mathcal{F}_q(t) = \begin{cases} 256t^2 & \text{if } N \text{ is even,} \\ 16 \left[1 + \cos\left(\frac{\pi}{N}\right)\right]^4 t^2 & \text{if } N \text{ is odd,} \end{cases} \quad (80)$$

i.e. it is independent of the parameter λ of the perturbation and grows quadratically in time. Only the QFI for odd N depends on N , and for large N it approaches the QFI for even N , which does not depend on N .

Even the FI discriminates between even and odd N , because of the ambiguity in choosing the highest energy eigenstate for odd N (see Appendix C 2). For even N $\mathcal{F}_c(t) = \mathcal{F}_q(t)$, thus the position measurement is optimal. For odd N , the FI depends on the choice of the highest energy state. Both the eigenstates for $n = (N \pm 1)/2$ in Table I lead to $\mathcal{F}_c(t) = \mathcal{F}_q(t)$. Instead, if we choose the linear combinations of them in Eqs. (14)–(15), the FI of position measurement is no longer optimal, as shown in Fig. 17.

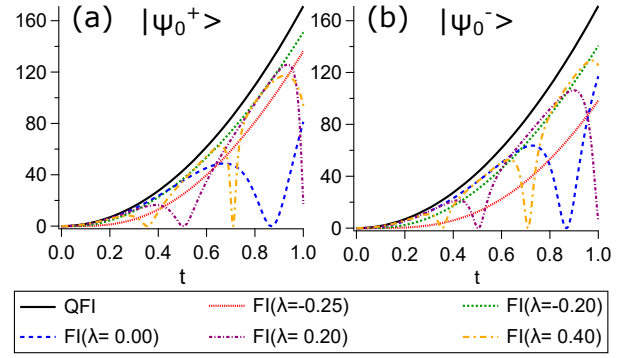


FIG. 17: Quantum (black solid line) and classical Fisher Information (colored non-solid lines) of position measurement for the states maximizing the QFI in the cycle graph for odd N : (a) $|\psi_0^+\rangle$, where the highest energy state is Eq. (14); and (b) $|\psi_0^-\rangle$, where the highest energy state is Eq. (15). Indeed, the highest energy level is doubly degenerate. While the QFI does not depend on the choice of the highest energy state, the FI does. In particular, the FI is equal to the QFI when we choose the highest energy state by definition (Table I). Instead, when we choose Eq. (14) or (15), the FI never reaches the QFI. Results for $N = 5$.

2. Complete graph

The complete graph has two distinct energy levels, and a possible choice of the state maximizing the QFI (at $t = 0$) is the following

$$|\psi_0^l\rangle = \frac{1}{\sqrt{2}}(|e_0\rangle + |e_1^l\rangle), \quad (81)$$

where $|e_0\rangle$ is the ground state, corresponding to the eigenvalue $\varepsilon_0 = 0$, while $|e_1^l\rangle$, with $l = 1, \dots, N-1$, is the eigenstate corresponding to the highest energy level $\varepsilon_1 = N$, which is $(N-1)$ -degenerate (see Table II). Then, we are free to choose any eigenstate from the eigenspace $\{|e_1^l\rangle\}$ (or even a superposition of them) and the QFI will be always

$$\mathcal{F}_q(N, t) = N^4 t^2. \quad (82)$$

The QFI is independent of the parameter λ , is quadratic in time, and it is $\mathcal{O}(N^4)$, thus greater than the QFI for a localized state, see Eq. (65).

On the other hand, the position Fisher Information does depend on the choice of $|e_1^l\rangle$. As an example, let us consider the two states

$$|\psi_0^1\rangle = \frac{1}{\sqrt{2}}(|e_0\rangle + |e_1^1\rangle), \quad (83)$$

$$|\psi_0^{N-1}\rangle = \frac{1}{\sqrt{2}}(|e_0\rangle + |e_1^{N-1}\rangle), \quad (84)$$

which are equivalent from the point of view of the QFI (both maximize it), but they are not from that of the FI (see Fig. 18). Indeed, such states lead to the following

FI

$$\mathcal{F}_c(|\psi_0^1\rangle; N, t, \lambda) = \frac{4t^2 N^4 (N+2) \sin^2(2t\omega_N(\lambda))}{(N+2)^2 - 8N \cos^2(2t\omega_N(\lambda))}, \quad (85)$$

$$\mathcal{F}_c(|\psi_0^{N-1}\rangle; N, t, \lambda) = \frac{4(N-1)N^4 t^2 \sin^2(2t\omega_N(\lambda))}{N^2 - 4(N-1) \cos^2(2t\omega_N(\lambda))}. \quad (86)$$

In both cases the FI is symmetric with respect to $\lambda^* = -1/N$, and for such value it vanishes. The local maxima occur for $t_k = \pi(k + 1/2)/(N + \lambda N^2)$, with $k \in \mathbb{N}$, and are

$$\mathcal{F}_c^{max}(|\psi_0^1\rangle; N, t_k, \lambda) = \frac{4N^4}{N+2} t_k^2, \quad (87)$$

$$\mathcal{F}_c^{max}(|\psi_0^{N-1}\rangle; N, t_k, \lambda) = 4(N-1)N^2 t_k^2. \quad (88)$$

For these superpositions the FI never reaches the value of the QFI (82), so performing a position measurement on $|\psi_0^l\rangle$ is not an optimal measurement.

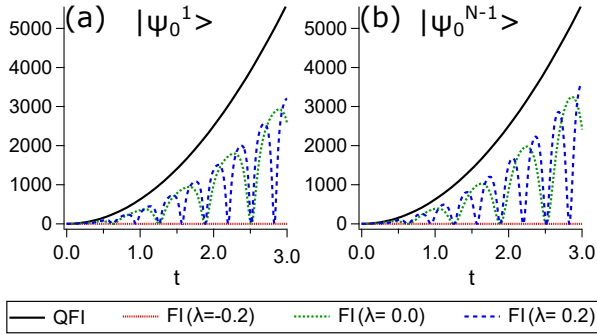


FIG. 18: Quantum (black solid line) and classical Fisher Information (colored non-solid lines) of position measurement for two of the states maximizing the QFI in the complete graph: (a) $|\psi_0^1\rangle$ and (b) $|\psi_0^{N-1}\rangle$. Indeed, due to the degeneracy of the highest energy level, there exist several states providing the same maximum QFI. While the QFI does not depend on the choice of such states, the FI does. In both cases, the FI vanishes for $\lambda^* = -1/N = -0.2$. Results for $N = 5$.

3. Star graph

In the star graph the state maximizing QFI (at $t = 0$) is

$$|\psi_0\rangle = \frac{1}{\sqrt{2}}(|e_0\rangle + |e_2\rangle), \quad (89)$$

where $|e_0\rangle$ is the ground state, corresponding to the eigenvalue $\varepsilon_0 = 0$, while $|e_2\rangle$ is the eigenstate corresponding to the highest energy level $\varepsilon_2 = N$ (see Table III). The resulting QFI

$$\mathcal{F}_q(N, t) = N^4 t^2 \quad (90)$$

is equal to that of the complete graph, because of the same eigenvalues involved (see Eq. (82)). The QFI is

independent of the parameter λ , is quadratic in time, and it is $\mathcal{O}(N^4)$, thus greater than the QFI for a localized state, see Eq. (68).

Since the highest energy level is not degenerate, there is no ambiguity in the state maximizing the QFI. For such state the FI reads as

$$\mathcal{F}_c(N, t, \lambda) = \frac{4(N-1)N^4 t^2 \sin^2(2t\omega_N(\lambda))}{N^2 - 4(N-1) \cos^2(2t\omega_N(\lambda))}, \quad (91)$$

which exactly matches with Eq. (86), so please also refer to Fig. 18(b). The FI is symmetric with respect to $\lambda^* = -1/N$, and for such value it vanishes. The local maxima are (88), so the FI for these states never equals the QFI (90).

C. General Graph

In this section we prove that for a specific class of graphs the maximum QFI is always equal to $N^4 t^2$, provided that the probe of the system is the one given by the Parthasarathy's Lemma 1, i.e. the state (75). Indeed, according to this lemma, in order to find quantum probes maximizing the QFI, we need to search for systems whose eigenvalues separation is maximum. For a graph of N vertices with no loops, the row sums and the column sums of the graph Laplacian L_N are all equal to 0 and the vector $(1, \dots, 1)$ is always an eigenvector of L with eigenvalue 0. It follows that any Laplacian spectrum contains the zero eigenvalue and to maximize the QFI we need to find graphs having the largest maximum eigenvalue.

Following Ref. [54], the Laplacian spectrum of a graph $G(V, E)$ is the set of the eigenvalues of L_N

$$S_L(G) = \{\mu_1 = 0, \mu_2, \dots, \mu_N\}, \quad (92)$$

where the eigenvalues μ_i are sorted in ascending order. To study the maximum eigenvalue μ_N we introduce the complementary graph \bar{G} of G . The complementary graph \bar{G} is defined on the same vertices of G and two distinct vertices are adjacent in \bar{G} if and only if they are not adjacent in G . So, the adjacency matrix \bar{A} can be straightforwardly derived from A by replacing all the off-diagonals 0s with 1s and all the 1s with 0s. In other words

$$\bar{A}_N = \mathbb{J}_N - \mathbb{1}_N - A_N, \quad (93)$$

where \mathbb{J}_N denotes the $N \times N$ all-ones matrix and $\mathbb{1}_N$ the $N \times N$ identity matrix. A vertex in G can be at most adjacent to $N - 1$ vertices, since no loops are allowed. Then, the degree \bar{d}_j of a vertex in \bar{G} is $N - 1 - d_j$, i.e. the complement to $N - 1$ of the degree of the same vertex in G . The diagonal degree matrix is therefore

$$\bar{D}_N = (N - 1)\mathbb{1}_N - D_N. \quad (94)$$

In conclusion, the Laplacian matrix \bar{L}_N associated to \bar{G} is

$$\bar{L}_N = \bar{D}_N - \bar{A}_N = N\mathbb{1}_N - \mathbb{J}_N - L_N. \quad (95)$$

Ref. [54] reports the following result, of which we offer an explicit proof.

Lemma 2. *Any eigenvector \vec{n} of L_N is an eigenvector of \bar{L}_N . If the eigenvalue of \vec{n} for L_N is 0, then it is 0 also for \bar{L}_N . If the eigenvalue of \vec{n} for L_N is μ_i , then the eigenvalue for \bar{L}_N is $N - \mu_i$. Thus, the spectrum of \bar{L}_N is given by*

$$S_{\bar{L}}(\bar{G}) = \{0, N - \mu_N, \dots, N - \mu_2\}, \quad (96)$$

where the eigenvalues are still sorted in ascending order.

Proof. Let $\vec{n} = (n_1, \dots, n_N)$ be the generic eigenvector of L_N . Since every row sum and column sum of L_N is zero, there are two kinds of eigenvector.

- (i) The first eigenvector is $n_1 = \dots = n_N = 1$ with eigenvalue $\mu_1 = 0$, so $\mathbb{J}_N \vec{n} = N \vec{n}$. Then

$$\bar{L}_N \vec{n} = (N \mathbb{1}_N - \mathbb{J}_N - L_N) \vec{n} = 0, \quad (97)$$

i.e. the eigenvector of L_N with eigenvalue $\mu_1 = 0$ is an eigenvector of \bar{L} with same eigenvalue.

- (ii) The other eigenvectors, whose eigenvalues μ_i can be different from 0, must be orthogonal to the first one. In other words, these eigenvectors must satisfy the condition $\sum_{i=1}^N n_i = 0$, so $\mathbb{J}_N \vec{n} = 0$. Then

$$\bar{L}_N \vec{n} = (N \mathbb{1}_N - \mathbb{J}_N - L_N) \vec{n} = (N - \mu) \vec{n}, \quad (98)$$

i.e. the eigenvector of L_N with eigenvalue μ_i is an eigenvector of \bar{L}_N with eigenvalue $N - \mu_i$.

□

Any L_N is positive-semidefinite [54], i.e. $\mu_i \geq 0 \forall i$, so this holds for \bar{L}_N too. Considering $S_{\bar{L}}(\bar{G})$, it follows that $\mu_N \leq N$, i.e. the largest eigenvalue is bounded from above by the number of vertices N . Moreover, the second-smallest eigenvalue μ_2 of L_N is the algebraic connectivity of G : it is greater than 0 if and only if G is a connected graph. Indeed, the algebraic multiplicity of the eigenvalue 0 is the number of connected components of the graph [55–57]. Then, the largest eigenvalue of L_N is $\mu_N = N$ if the complementary graph \bar{G} is disconnected. Indeed, if \bar{G} has at least two distinct components, then the second-smallest eigenvalue of \bar{L}_N is $N - \mu_N = 0$.

Lemma 3. *Given a graph G and its Laplacian spectrum $S_L(G) = \{0, \mu_2, \dots, \mu_N\}$, the largest laplacian eigenvalue μ_N is bounded from above by*

$$\mu_N \leq N, \quad (99)$$

and the equality is saturated only if the complementary graph \bar{G} is disconnected.

This result in spectral graph theory has a direct impact on our estimation problem. Since our perturbation is the square of the graph Laplacian, the maximum QFI is given by Eq. (77) and involves the lowest and the greatest eigenvalue of the Laplacian spectrum. Hence, we obtain the following lemma.

Lemma 4. *The simple graphs G whose complementary graph \bar{G} is disconnected are the only ones providing the maximum QFI for the estimate of the parameter λ in Eq. (1). For such graphs, the largest eigenvalue of the graph Laplacian is N and the lowest is 0. This results in the following maximum QFI*

$$\mathcal{F}_q^{max}(N, t) = t^2 N^4. \quad (100)$$

This lemma allows us to predict whether or not a graph will maximize the QFI and which value the QFI will take, with no need to diagonalize its Laplacian. Both the complete graph, whose \bar{G} has N disconnected components, and the star graph, whose \bar{G} has 2 disconnected components, provide the maximum QFI (100), as proved in Sec. IIIB 2 and Sec. IIIB 3, respectively. Other examples of graphs satisfying the Lemma 4 are the wheel graph (the union of a N -star and a $(N - 1)$ -cycle) and the complete bipartite graph.

In Sec. IIIB 1 we have proved that the cycle graph has a different maximum QFI, see Eq. (80). The spectrum of the Laplacian is shown in Table I. As expected, the minimum eigenvalue $\mu_1 = 0$, but the maximum eigenvalue $\mu_N = 4$ is for even N . This value saturates Eq. (99) if and only if $N = 4$. Indeed, the complementary graph of the cycle with 4 vertices has two disconnected components. Thus the 4-cycle satisfies the Lemma 4 and provides the QFI (100). Instead, for $N > 4$ the complementary graph of the cycle graph is connected and the resulting QFI is always lower than (100). For $N = 2$ and $N = 3$ the cycle graph is nothing but a complete graph, which we can refer to for the results.

IV. DISCUSSION AND CONCLUSIONS

In this paper we have investigated the dynamics and the characterization of continuous-time quantum walks (CTQW) with Hamiltonians of the form $\mathcal{H} = L + \lambda L^2$, being L the Laplacian (Kirchoff) matrix of the underlying graph. In particular, we have paid attention to CTQW on cycle, complete, and star graphs, as they describe paradigmatic models with low/high connectivity and/or symmetry. In the following we summarize and discuss our results, starting from the dynamical aspects.

On the cycle graph the probability distribution over the sites is symmetric with respect to the starting vertex and involves sums of cosine functions, with the quadratic term in the Hamiltonian affecting their angular frequencies. We have numerically evaluated the probability and, in the considered time interval, our results suggest the presence of revivals in the initial vertex. On the other hand, revivals are not exact given the incommensurability of the periods of the cosine functions. We have also considered the variance of the position, and as long as the tails of the wavefunction do not meet each other in the vertex opposite to the initial one, the spreading

	QFI			FI		
	<i>cycle</i>	<i>complete</i>	<i>star</i>	<i>cycle</i>	<i>complete</i>	<i>star</i>
<i>Localized states</i>	$\mathcal{O}(1)$	$\mathcal{O}(N^3)$	$\mathcal{O}(N^2)$	$\mathcal{O}(1)$	$\mathcal{O}(N^3)$	$\mathcal{O}(N^2)$
<i>Maximum QFI states</i>	$\mathcal{O}(1)$	$\mathcal{O}(N^4)$	$\mathcal{O}(N^4)$	$\mathcal{O}(1)$	$\mathcal{O}(N^3)$	$\mathcal{O}(N^3)$

TABLE IV: Asymptotic behavior of the quantum Fisher information and of the classical Fisher information for large size N of the cycle, complete, and star graphs, for localized and maximum QFI states.

	FI		
	<i>cycle</i>	<i>complete</i>	<i>star</i>
<i>Localized states</i>	$\mathcal{O}(t^2)$	$\mathcal{O}(t^2)$	$\mathcal{O}(t^2)$
<i>Maximum QFI states</i>	$\mathcal{O}(t^2)$ for energy eigenstates in Table I $\mathcal{O}(t^4)$ for odd N and highest energy eigenstate (14) or (15)	$\mathcal{O}(t^4)$	$\mathcal{O}(t^4)$

TABLE V: Behavior at short times t of the classical Fisher information of the cycle, complete, and star graphs, for localized and maximum QFI states. The maximum QFI state is the superposition of the ground state and the highest energy eigenstate. The QFI is always $\mathcal{O}(t^2)$, even at short and long times, as can be seen from Eq. (63), since the perturbation \mathcal{H}_1 is time-independent.

is ballistic independently of the perturbation. Indeed, in this regime, we have $\sigma^2(t) = [40(\lambda - \lambda_0)^2 + 2/5]t^2$, where $\lambda_0 = -1/5$ is the value at which the next-nearest-neighbor hopping equals the nearest-neighbor hopping. The variance is therefore symmetric with respect to λ_0 and the perturbation only affects the speed of the walker through the prefactor. Numerical results also suggest that instantaneous uniform mixing is not achievable for $N > 4$. On the other hand, the average probability distribution approaches the uniform one for large N . These findings are consistent with the results from the inverse participation ratio (IPR), where the numerical results show that there is no complete localization for $t > 0$, confirming the absence of exact revivals. Finally, upon evaluating the coherence for short times, we found that it has a minimum for $\lambda = -1/4$, for which the nearest-neighbor hopping amplitude vanishes, and the next-nearest-neighbor hopping one does not.

In the complete graph all the vertices are equivalent, and the probability distribution shows exact revivals in the initial vertex. For large N the walker is strongly localized in the initial vertex and the probability distribution is symmetric with respect to $\lambda^* = -1/N$, which is the value for which the angular frequency appearing in the distribution vanishes. Exact instantaneous mixing is achievable only for $N = 2, 3, 4$, whereas the average probability distribution is never close to the uniform one, except for $N = 2$. These findings are consistent with the results from the IPR, which is periodic in time. Moreover, the larger N , the more localized is the walker. Also coherence is periodic, and it vanishes for $\lambda = \lambda^*$.

For the star graph, when the initial vertex is the central one, the dynamics is equivalent to the dynamics of an initially localized walker in a complete graph of the

same size. For this reason, we have focused attention to a walker initially localized in an outer vertex. The probability distribution shows revivals in the initial vertex, and for large N the walker is strongly localized in the initial vertex. Whether the revivals are exact or not, it depends on the size of the graph and on λ . The instantaneous exactly uniform mixing is only achievable for $2 \leq N \leq 4$ and it strongly depends on the choice of (N, λ) . The average probability distribution is never close to the uniform one, except for $N = 2$. These findings are consistent with the results from the IPR, where, analogously to the complete graph, the larger is N , the more localized is the walker. The coherence is characterized by a complex structure of local maxima e minima. However, it is periodic and smoother for the values of λ which make the overall probability distribution periodic (see Eq. (B32) in Appendix B 3).

Concerning characterization, we have addressed the optimal estimation of the parameter λ by evaluating the quantum Fisher information (QFI) and the Fisher information (FI) of position measurements, both for localized states and for states maximizing the QFI. Upon exploiting Parthasarathy's lemma we have found that states maximizing the QFI are equally-weighted linear combination of the eigenstates corresponding to the minimum and maximum eigenvalues of the perturbation. Moreover, we have found that the simple graphs whose complementary graph is disconnected are the only ones providing the maximum QFI $\mathcal{F}_q^{max}(N, t) = N^4 t^2$. For the others graph, we sum up the asymptotic behavior of the (Q)FI for large N in Table IV and for $t \ll 1$ in Table V.

For the cycle graph, the QFI of a localized state is quadratic in time and independent of the perturbation and of the size N of the graph. The FI of position mea-

surement shows local maxima in which it is close to the QFI. On the other hand, the QFI for the optimal states is quadratic in time, independent of the perturbation, but it does depend on N . For even N , the FI is optimal, i.e. it equals the QFI. For odd N , the highest energy level is doubly degenerate. The FI is optimal when the state maximizing the QFI involves one of the two eigenstates corresponding to the highest energy level, but the FI is no longer optimal when considering a linear combination of these two.

For the complete graph, the QFI of a localized state is again quadratic in time, it scales as $\mathcal{O}(N^3)$ with the size of the graph, and it is independent of the perturbation. The FI of position measurement is symmetric with respect to the value $\lambda^* = -1/N$, and the periodicity of the probability distribution leads to oscillations in the FI, which grow in time. The local maxima of the FI equal the QFI, i.e. there are instants of time in which the position measurement is optimal. This happens when the walker is exactly localized in the initial vertex. Indeed, knowing when the walker is back corresponds to knowing exactly its period, and thus the parameter λ . The minima of the FI, instead, are equal to 0. The QFI of the optimal states is quadratic in time, scales as $\mathcal{O}(N^4)$ (greater than the QFI for the localized state), and it is independent of the perturbation. The highest energy level is $(N - 1)$ -degenerate, and therefore the FI depends on the choice of the corresponding eigenstate in the optimal state. We have considered two different eigenstates $|e_1^1\rangle$ and $|e_1^{N-1}\rangle$, and the resulting FI shows an oscillating behavior which amplifies in time. However, its local maxima do not match the curve of the QFI. The FI is symmetric with respect to $\lambda^* = -1/N$, and it vanishes for such value.

For the star graph, the QFI of a localized state (outer vertex) is quadratic in time, scales as $\mathcal{O}(N^2)$, and it is independent of the perturbation. The FI of position measurements shows an oscillating behavior, which amplifies in time. However, the local maxima of the FI do not match the QFI. The QFI of the optimal state is equal to that of the complete graph, i.e. it is quadratic in time, scales as $\mathcal{O}(N^4)$ (greater than the QFI for the localized state), and it is independent of the perturbation. The highest energy level is not degenerate, so there is no ambiguity in the state maximizing the QFI. For such state, the FI turns out to be equal to that of the state involving $|e_1^{N-1}\rangle$ in the complete graph.

In conclusion, in this paper we have discussed in details the dynamics and the characterization of continuous-time quantum walks (CTQW) in the presence of a quadratic perturbation, i.e. governed by Hamiltonians of the form $\mathcal{H} = L + \lambda L^2$, where L is the Laplacian matrix of the underlying graph. We have discussed the properties of CTQW on cycle, complete and star graphs as they represent paradigmatic examples of simple graphs with low/high connectivity and/or symmetry. Our results indicate the general quantum features of CTQWs on graphs, e.g. ballistic spreading, revivals, interference

and creation of coherence are still present in their perturbed versions. On the other hand, novel interesting effects emerge, such as the dependence of the speed of the walker on the perturbation amplitude λ , and the appearance of symmetries in the behavior of coherence and localization, due to the trade-off between nearest-neighbor and next-nearest-neighbor hopping amplitudes. Besides fundamental interest, our detailed analysis may find applications in the design of enhanced algorithms on graphs, and as a necessary ingredient to study dephasing and decoherence.

Acknowledgments

This study has been partially supported by SERB through the VAJRA scheme (grant VJR/2017/000011). P.B. and M.G.A.P. are members of GNFM-INdAM.

Appendix A: Origin of the perturbation λL^2 for the cycle graph

In this appendix we show that modeling the perturbation as the square of the graph Laplacian for the cycle graph naturally arises from the spatial discretization of the Hamiltonian, in the continuum, having a perturbation in \hat{p}^4 .

To begin with, we consider an infinite line, i.e. a one-dimensional lattice of equally spaced sites (lattice parameter d). Being the space discretized, we approximate the spatial derivatives as finite differences [58]:

$$\frac{\partial^2 f_n}{\partial x^2} = \frac{1}{d^2}(f_{n+1} - 2f_n + f_{n-1}) + \mathcal{O}(d^2), \quad (\text{A1})$$

$$\frac{\partial^4 f_n}{\partial x^4} = \frac{1}{d^4}(f_{n+2} - 4f_{n+1} + 6f_n - 4f_{n-1} + f_{n-2}) + \mathcal{O}(d^2). \quad (\text{A2})$$

The Hilbert space of our system is spanned by the position states $\{|n\rangle | n \in \mathbb{Z}\}$. The position states form an orthonormal basis, on which the generic state is expanded as $|\psi\rangle = \sum_n \psi_n |n\rangle$. Since the differential operators act on the wavefunction $\psi_n = \langle n|\psi\rangle$ [59] according to Eqs. (A1)–(A2), it follows that the unperturbed Hamiltonian is

$$\mathcal{H}_0 = -\gamma \left[\sum_n (|n-1\rangle\langle n| + |n+1\rangle\langle n|) - 2I \right], \quad (\text{A3})$$

while the perturbation due to gravity corrections (see

Sec. I) is

$$\begin{aligned}\lambda\mathcal{H}_1 &:= \frac{\beta}{m}p_0^4 \\ &= -\gamma\lambda \left[\sum_n (-|n-2\rangle\langle n| + 4|n-1\rangle\langle n| \right. \\ &\quad \left. + 4|n+1\rangle\langle n| - |n+2\rangle\langle n|) - 6I \right],\end{aligned}\quad (\text{A4})$$

with $I = \sum_n |n\rangle\langle n|$ the identity. We define the hopping amplitude

$$\gamma := -\frac{\hbar^2}{2md^2}, \quad (\text{A5})$$

and the dimensionless real parameter

$$\lambda := \frac{2\beta\hbar^2}{d^2}. \quad (\text{A6})$$

Then, the total Hamiltonian $\mathcal{H} = \mathcal{H}_0 + \lambda\mathcal{H}_1$ reads as

$$\begin{aligned}\mathcal{H} = -\gamma \left\{ \sum_n [-\lambda|n+2\rangle\langle n| + (1+4\lambda)|n+1\rangle\langle n| \right. \\ \left. + (1+4\lambda)|n-1\rangle\langle n| - \lambda|n-2\rangle\langle n|] - (2+6\lambda)I \right\}.\end{aligned}\quad (\text{A7})$$

The perturbation \mathcal{H}_1 affects the nearest-neighbor hopping (which is proper of the unperturbed Hamiltonian \mathcal{H}_0), the on-site energies $\propto I$, and introduces the next-nearest-neighbor hopping.

Now we refine the Hamiltonian in Eq. (A7) for the cycle graph (Fig. 1(a)) and set $\gamma = 1$. A cycle graph, indeed, can be thought as a finite line of N sites, indexed from 0 to $N-1$, with periodic boundary conditions (PBC), that is $|n \pm M\rangle := |(n \pm M) \bmod N\rangle$, with $M \in \mathbb{N}$. The unperturbed Hamiltonian is

$$\begin{aligned}\mathcal{H}_0 = \sum_{n=0}^{N-1} [-(1-\delta_{n,N-1})|n+1\rangle\langle n| \\ -(1-\delta_{n,0})|n-1\rangle\langle n|] + 2I + \mathcal{B}_0.\end{aligned}\quad (\text{A8})$$

The terms related to $|n \pm 1\rangle\langle n|$ are accountable for the hopping within the line and prevent the walker from getting out of the line, e.g., $(1-\delta_{N-1,N-1})|N\rangle\langle N-1| = 0$. On the other hand, the term

$$\mathcal{B}_0 := -|N-1\rangle\langle 0| - |0\rangle\langle N-1| \quad (\text{A9})$$

encodes the PBC. The matrix representation of this Hamiltonian is the graph Laplacian of the cycle graph in Eq. (7).

The perturbation is

$$\begin{aligned}\mathcal{H}_1 = \sum_{n=0}^{N-1} [(1-\delta_{n,N-1})(1-\delta_{n,N-2})|n+2\rangle\langle n| \\ - 4(1-\delta_{n,N-1})|n+1\rangle\langle n| - 4(1-\delta_{n,0})|n-1\rangle\langle n| \\ + (1-\delta_{n,0})(1-\delta_{n,1})|n-2\rangle\langle n|] + 6I + \mathcal{B}_1,\end{aligned}\quad (\text{A10})$$

where again the former terms are accountable for the hopping within the line and

$$\mathcal{B}_1 := 4\mathcal{B}_0 + |N-2\rangle\langle 0| + |0\rangle\langle N-2| + |N-1\rangle\langle 1| + |1\rangle\langle N-1| \quad (\text{A11})$$

encodes the PBC. Its matrix representation is

$$\mathcal{H}_1 = \begin{pmatrix} 6 & -4 & 1 & 0 & \cdots & \cdots & 0 & 1 & -4 \\ -4 & 6 & -4 & 1 & \ddots & & & \ddots & 1 \\ 1 & -4 & \ddots & \ddots & \ddots & \ddots & & & 0 \\ 0 & 1 & \ddots & \ddots & \ddots & \ddots & \ddots & & \vdots \\ \vdots & \ddots & \ddots & \ddots & \ddots & \ddots & \ddots & \ddots & \vdots \\ \vdots & & \ddots & \ddots & \ddots & \ddots & \ddots & 1 & 0 \\ 0 & & & \ddots & \ddots & \ddots & \ddots & -4 & 1 \\ 1 & \ddots & & & \ddots & 1 & -4 & 6 & -4 \\ -4 & 1 & 0 & \cdots & \cdots & 0 & 1 & -4 & 6 \end{pmatrix}, \quad (\text{A12})$$

and it is symmetric and circulant. One can easily check that the square of Eq. (7) returns Eq. (A12). Alternatively, one can prove it by explicitly considering the Hamiltonians in Eq. (A8) and Eq. (A10).

Appendix B: Analytical derivation of the results for the dynamics

The dynamics of the system is essentially encoded in the time evolution of the density matrix. For an initially localized state $|j\rangle$, the density matrix is given by $\rho(t) = |j(t)\rangle\langle j(t)|$, whose generic element in the position basis is

$$\rho_{m,n}(t) = \langle m|\mathcal{U}_\lambda(t)|j\rangle\langle j|\mathcal{U}_\lambda^\dagger(t)|n\rangle, \quad (\text{B1})$$

where the time-evolution operator $\mathcal{U}_\lambda(t)$ is defined in Eq. (2).

The probability distribution as a function of time is given by the diagonal elements of the density matrix:

$$P_j(i, t|\lambda) = |\langle i|j(t)\rangle|^2 = \langle i|j(t)\rangle\langle j(t)|i\rangle = \rho_{i,i}(t). \quad (\text{B2})$$

The modulus of the off-diagonal elements of the density matrix entering the definition of coherence in Eq. (6) can also be expressed in terms of probabilities:

$$\begin{aligned}|\rho_{m,n}(t)| &= |\langle m|\mathcal{U}_\lambda(t)|j\rangle\langle n|\mathcal{U}_\lambda(t)|j\rangle| \\ &= \sqrt{P_j(m, t|\lambda)P_j(n, t|\lambda)} = |\rho_{n,m}(t)|,\end{aligned}\quad (\text{B3})$$

where the probabilities are provided in Eq. (B2).

1. Cycle Graph

First, we prove the symmetry with respect to the starting vertex j of the probability distribution in Eq. (17),

i.e. $P_j(j+k, t|\lambda) = P_j(j-k, t|\lambda)$. The left-hand side of this equation is

$$P_j(j+k, t|\lambda) = \frac{1}{N^2} \sum_{n,m=0}^{N-1} e^{-i(E_n^\lambda - E_m^\lambda)t} e^{i\frac{2\pi}{N}(n-m)(-k)}. \quad (\text{B4})$$

Now, letting $l = N - n$ ($q = N - m$) be the new summation indices, and since $\varepsilon_{N-l} = \varepsilon_l$ ($\varepsilon_{N-q} = \varepsilon_q$), we have that

$$\begin{aligned} P_j(j+k, t|\lambda) &= \frac{1}{N^2} \sum_{l,q=1}^N e^{-i(E_l^\lambda - E_q^\lambda)t} e^{i\frac{2\pi}{N}(q-l)k} \\ &= \frac{1}{N^2} \sum_{l,q=0}^{N-1} e^{-i(E_l^\lambda - E_q^\lambda)t} e^{i\frac{2\pi}{N}(l-q)[j-(j-k)]} \\ &= P_j(j-k, t|\lambda), \end{aligned} \quad (\text{B5})$$

The second equality holds since the summand of index $l = N$ ($q = N$) is equal to that of index $l = 0$ ($q = 0$). Indeed, according to Table I, the virtual E_N^λ is equal to E_0^λ (the actual energies have index running from 0 to $N-1$). In addition, $\exp\{i\frac{2\pi}{N}(q-l)k\}$ returns the same value if evaluated in $l = N$ ($q = N$) or $l = 0$ ($q = 0$).

Instead, deriving the average probability distribution in the cycle graph requires some expedients. The instantaneous probability distribution is provided in Eq. (17), and the average one follows from Eq. (4). Since the summations are over a finite number of terms, we may interchange the limit and the integral operations with the summations, i.e.

$$\bar{P}_j(k|\lambda) = \frac{1}{N^2} \sum_{m,n=0}^{N-1} e^{i\frac{2\pi}{N}(n-m)(k-j)} I_{nm}, \quad (\text{B6})$$

where

$$I_{nm} := \lim_{T \rightarrow +\infty} \frac{1}{T} \int_0^T e^{-i(E_n^\lambda - E_m^\lambda)t} dt. \quad (\text{B7})$$

The issue of evaluating such quantity is related to the degeneracy of the distinct energy levels $\{\varepsilon_n\}$ defining $E_n^\lambda := \varepsilon_n + \lambda \varepsilon_n^2$ (see Table I). Moreover, we have to distinguish even and odd N .

Even N For even N , there are $N/2+1$ distinct energy levels. The ground state $n = 0$ and the highest energy state $n = N/2$ are unique, whereas the remaining energy levels have degeneracy 2. Then, for a given n

$$I_{n,m} = \begin{cases} 1 & \text{if } m = n = 0 \vee m = n = N/2, \\ 1 & \text{if } (m = n \vee m = N - n) \wedge (n \neq 0, N/2), \\ 0 & \text{otherwise.} \end{cases} \quad (\text{B8})$$

The average probability distribution is therefore

$$\bar{P}_j(k|\lambda) = \frac{1}{N^2} \left[1 + 1 + \sum_{\substack{n=1, \\ n \neq N/2}}^{N-1} \left(1 + e^{i\frac{2\pi}{N}(2n-N)(k-j)} \right) \right]$$

$$\begin{aligned} &= \frac{1}{N^2} \left[2 + N - 2 + \sum_{n=1}^{N-1} e^{i\frac{4\pi n}{N}(k-j)} - e^{i2\pi(k-j)} \right] \\ &= \begin{cases} \frac{1}{N^2}(N + N - 1 - 1) & \text{if } k = j \\ \quad \vee k = j + N/2, \\ \frac{1}{N^2}(N - 1 - 1) & \text{otherwise,} \end{cases} \end{aligned} \quad (\text{B9})$$

from which Eq. (22) follows.

Odd N For odd N , there are $(N+1)/2$ distinct energy levels. The ground state $n = 0$ is unique, whereas the other energy levels have degeneracy 2. Then, for a given n

$$I_{n,m} = \begin{cases} 1 & \text{if } m = n = 0, \\ 1 & \text{if } (m = n \vee m = N - n) \wedge n \neq 0, \\ 0 & \text{otherwise.} \end{cases} \quad (\text{B10})$$

The average probability distribution is therefore

$$\begin{aligned} \bar{P}_j(k|\lambda) &= \frac{1}{N^2} \left[1 + \sum_{n=1}^{N-1} \left(1 + e^{i\frac{2\pi}{N}(2n-N)(k-j)} \right) \right] \\ &= \frac{1}{N^2} \left[1 + N - 1 + \sum_{n=1}^{N-1} e^{i\frac{4\pi n}{N}(k-j)} \right] \\ &= \begin{cases} \frac{1}{N^2}(N + N - 1) & \text{if } k = j, \\ \frac{1}{N^2}(N - 1) & \text{otherwise,} \end{cases} \end{aligned} \quad (\text{B11})$$

from which Eq. (23) follows.

2. Complete Graph

The complete graph has two energy levels (see Table II), thus the unitary time-evolution operator has the following spectral decomposition:

$$\mathcal{U}_\lambda(t) = |e_0\rangle\langle e_0| + e^{-2i\omega_N(\lambda)t} \sum_{l=1}^{N-1} |e_1^l\rangle\langle e_1^l|, \quad (\text{B12})$$

being $\omega_N(\lambda)$ defined in Eq. (31). By computing the matrix elements of this operator on the vertex states, we recover its matrix representation in the position basis (see Eq. (27)). Therefore, the time evolution of an initially localized state $|j\rangle$ is easily obtained as the j -th column of such matrix and is equal to Eq. (28). Knowing the state at a later time $t > 0$, we can determine the density matrix $\rho(t) = |j(t)\rangle\langle j(t)|$ in the position basis:

$$\rho(t) = \begin{pmatrix} \mathbb{A}_{j \times j} & \mathbb{B}_j^\dagger & \mathbb{A}_{j \times (N-j-1)} \\ \mathbb{B}_j & 1 - A(N-1) & \mathbb{B}_{N-j-1} \\ \mathbb{A}_{(N-j-1) \times j} & \mathbb{B}_{N-j-1}^\dagger & \mathbb{A}_{(N-j-1) \times (N-j-1)} \end{pmatrix}. \quad (\text{B13})$$

It is a block matrix where $\mathbb{A}_{m \times n} = A\mathbb{J}_{m \times n}$, $\mathbb{B}_n = B\mathbb{J}_{1 \times n}$ is a row vector, and

$$A = \frac{4}{N^2} \sin^2(\omega_N(\lambda)t), \quad (\text{B14})$$

$$B = \frac{4}{N^2} \sin^2(\omega_N(\lambda)t) + \frac{1}{N} \left(e^{-2it\omega_N(\lambda)} - 1 \right). \quad (\text{B15})$$

Then, we can evaluate the probability distribution $P_j(k, t|\lambda)$ according to Eq. (B2), which provides the results in Eqs. (29)–(30).

Lastly, the coherence of an initially localized state follows from Eq. (6) and (B13) and reads as

$$\begin{aligned} \mathcal{C}(\rho) &= 2(N-1)|B| + (N-1)(N-2)|A| \\ &= \frac{4(N-1)}{N} \left[\frac{N-2}{N} \sin^2(\omega_N(\lambda)t) \right. \\ &\quad \left. + \sqrt{\frac{4(1-N)}{N^2} \sin^4(\omega_N(\lambda)t) + \sin^2(\omega_N(\lambda)t)} \right]. \end{aligned} \quad (\text{B16})$$

3. Star graph

The star graph has three energy levels (see Table III), thus the unitary time-evolution operator has the follow-

ing spectral decomposition:

$$\begin{aligned} \mathcal{U}_\lambda(t) &= |e_0\rangle\langle e_0| + e^{-2it\omega_1} \sum_{l=1}^{N-2} |e_1^l\rangle\langle e_1^l| \\ &\quad + e^{-2it\omega_N} |e_2\rangle\langle e_2|, \end{aligned} \quad (\text{B17})$$

being $\omega_N(\lambda)$ defined in Eq. (31). Again, by computing the matrix elements of this operator on the vertex states, we recover its matrix representation in the position basis (see Eq. (40)). Therefore, the time evolution of an initially localized state $|j\rangle$ is easily obtained as the j -th column of such matrix and is equal to Eq. (43) for $j \neq 0$. Recall that for $j = 0$ results are the same of an initially localized vertex in the complete graph of the same size. Knowing the state at a later time $t > 0$, we can determine the density matrix $\rho(t) = |j(t)\rangle\langle j(t)|$ in the position basis:

$$\rho(t) = \begin{pmatrix} D & \mathbb{A}_{j-1}^\dagger & A^* + C^* & \mathbb{A}_{N-j-1}^\dagger \\ \mathbb{A}_{j-1} & \mathbb{B}_{(j-1) \times (j-1)} & \mathbb{F}_{j-1}^\dagger & \mathbb{B}_{(j-1) \times (N-j-1)} \\ A + C & \mathbb{F}_{j-1} & 1 + B + E + E^* & \mathbb{F}_{N-j-1} \\ \mathbb{A}_{N-j-1} & \mathbb{B}_{(N-j-1) \times (j-1)} & \mathbb{F}_{N-j-1}^\dagger & \mathbb{B}_{(j-1) \times (j-1)} \end{pmatrix}. \quad (\text{B18})$$

It is a block matrix where the sub-matrices are

$$\mathbb{A}_m = A\mathbb{J}_{m \times 1}, \quad (\text{B19})$$

$$\mathbb{B}_{m \times n} = B\mathbb{J}_{m \times n}, \quad (\text{B20})$$

$$\mathbb{F}_n = (B + E)\mathbb{J}_{1 \times n}, \quad (\text{B21})$$

and the scalar values are

$$A = \frac{1}{N(N-1)} \left[\frac{4}{N} \sin^2(t\omega_N(\lambda)) + e^{-2it(\omega_1(\lambda) - \omega_N(\lambda))} - e^{-2it\omega_N(\lambda)} \right], \quad (\text{B22})$$

$$B = \frac{4}{N(N-1)} \left[\frac{1}{N-1} \sin^2[t(\omega_1(\lambda) - \omega_N(\lambda))] + \sin^2(\omega_1(\lambda)t) - \frac{1}{N} \sin^2(\omega_N(\lambda)t) \right], \quad (\text{B23})$$

$$C = \frac{1}{N} e^{-2it\omega_1(\lambda)} \left[1 - e^{2it\omega_N(\lambda)} \right], \quad (\text{B24})$$

$$D = \frac{4}{N^2} \sin^2(t\omega_N(\lambda)), \quad (\text{B25})$$

$$E = e^{-2it\omega_1(\lambda)} \left[\frac{1}{N} + \frac{e^{2it\omega_N(\lambda)}}{N(N-1)} - \frac{e^{2it\omega_1(\lambda)}}{N-1} \right]. \quad (\text{B26})$$

Then, we can evaluate the probability distribution $P_j(k, t|\lambda)$ according to Eq. (B2), which provides the results in Eqs. (44)–(46).

It is still pending the question about the periodicity of the probability distribution. Ultimately, the overall probability distribution is periodic if and only if the periods of the sine functions involved by the probabilities (44)–(46) are commensurable. Since such sine functions are squared, the periods are:

$$T_1(\lambda) := \frac{\pi}{\omega_1(\lambda)} = \frac{2\pi}{1 + \lambda}, \quad (\text{B27})$$

$$T_N(\lambda) := \frac{\pi}{\omega_N(\lambda)} = \frac{2\pi}{N + \lambda N^2}, \quad (\text{B28})$$

$$T_{N,1}(\lambda) := \frac{\pi}{\omega_N(\lambda) - \omega_1(\lambda)} = \frac{2\pi}{(N-1)[1 + \lambda(N+1)]}, \quad (\text{B29})$$

being $\omega_N(\lambda)$ defined in Eq. (31). Two non-zero real numbers are commensurable if their ratio is a rational number. The idea is therefore to express both $T_1(\lambda)$ and $T_{N,1}(\lambda)$ as multiple integers of $T_N(\lambda)$. From the ratio $T_1(\lambda)/T_N(\lambda)$ we get

$$T_1(\lambda) = \frac{N(1 + \lambda N)}{1 + \lambda} T_N(\lambda) =: p_N^\lambda T_N(\lambda), \quad (\text{B30})$$

with $\lambda \neq -1 \wedge \lambda \neq -1/N$, and from $T_{N,1}(\lambda)/T_N(\lambda)$

$$T_{N,1}(\lambda) = \frac{N(1 + \lambda N)}{(N-1)[1 + \lambda(N+1)]} T_N(\lambda) =: q_N^\lambda T_N(\lambda), \quad (\text{B31})$$

with $\lambda \neq -1/N \wedge \lambda \neq -1/(N+1)$. Then, we need to find the value of λ such that $p_N^\lambda, q_N^\lambda \in \mathbb{N}$ at the same time. Combining the definition of p_N^λ and q_N^λ in Eqs. (B30)–(B31) we find that they are related to λ and N by

$$\lambda = \frac{p_N^\lambda - q_N^\lambda(N-1)}{q_N^\lambda(N^2-1) - p_N^\lambda}. \quad (\text{B32})$$

Please notice that Eq. (B32) should always be intended together with Eqs. (B30)–(B31). As an example, for

$p_N^\lambda = q_N^\lambda$ we get $\lambda = (2 - N)/(N^2 - 2)$. However, the period must be unique, so we can not choose any $p_N^\lambda = q_N^\lambda$. Indeed, for such value of λ we get $p_N^\lambda = q_N^\lambda = 2$. In the end, by considering the least common multiple of the latter two integers, the total period of the probability distribution is

$$T = \text{lcm}(p_N^\lambda, q_N^\lambda) T_N(\lambda). \quad (\text{B33})$$

To define the above ratios (B30)–(B31) between the different periods, we have discarded the values $\lambda = -1, -1/N, -1/(N+1)$ because they make ω_1 , ω_N , and $\omega_N - \omega_1$ to vanish, respectively. However, for such values the overall probability distribution is actually periodic. To see this explicitly, let $p, q \in \mathbb{Z}$, and see that we can recover them from Eq. (B32) for $q = 0$, $q = -p$, and $p = 0$, respectively. Indeed, since these values of λ lead to vanishing angular frequency, the corresponding sine functions are vanishing too, and a constant function is trivially periodic (see Eqs. (44)–(46)).

Lastly, the coherence of an initially localized state $|j \neq 0\rangle$ follows from Eq. (6) and it requires the modulus of the off-diagonal elements of the density matrix. We can compute them as the modulus of the elements in Eq. (B18) or by exploiting their definition in Eq. (B3), where the probabilities $P_j(n, t|\lambda)$ are provided in Eqs. (44)–(46). Given the counting of the different matrix elements, and since $|\rho_{m,n}(t)| = |\rho_{n,m}(t)|$, the coherence reads as

$$\begin{aligned} \mathcal{C}(\rho) = & 2|A + C| + 2(N-2)|B + E| \\ & + 2(N-2)|A| + (N^2 - 5N + 6)|B|, \end{aligned} \quad (\text{B34})$$

where the number that multiplies $|B|$ follows from the fact that a $N \times N$ matrix has a total of $N^2 - N$ off-diagonal elements.

Appendix C: Fisher Information and Quantum Fisher Information for localized states and states maximizing the QFI

In this appendix we prove the analytical results about the relation between the Quantum Fisher Information (58) and the Fisher Information (59) in the different graphs. We provide the Fisher Information for a local position measurement whose POVM is given by $\{|0\rangle\langle 0|, |1\rangle\langle 1|, \dots, |N-1\rangle\langle N-1|\}$, i.e. by the projectors on the vertex states. The Parthasarathy's lemma 1 leads to the QFI in Eq. (82), because the state maximizing the QFI involves the ground state and the highest energy eigenstate. The highest energy level might be degenerate, but choosing any eigenstate of such level results in the same QFI. Instead, the Fisher information does depend on the choice of the highest energy eigenstate involved.

1. Alternative proof of the maximum QFI

We can also prove the formula of the QFI in Eq. (77) by approximating Eq. (76).

Proof. Let us assume that $[\mathcal{H}_0, \mathcal{H}_1] = 0$ and let $\{\epsilon_n\}$ be the eigenvalues of \mathcal{H}_1 . We take advantage of the relation between the eigenvalues of \mathcal{H}_1 and those of the unitary operator in Eq. (71). Indeed, in the limit for $\delta\lambda t \rightarrow 0$ we have that

$$\begin{aligned} \mathcal{F}_q(t) &= \frac{8}{\delta\lambda^2} \left[1 - \sqrt{\min_{i \neq j} \cos^2 \left(\frac{\delta\lambda t (\epsilon_i - \epsilon_j)}{2} \right)} \right] \\ &\approx \frac{8}{\delta\lambda^2} \left[1 - \sqrt{\min_{i \neq j} \left(1 - \frac{\delta\lambda^2 t^2}{4} (\epsilon_i - \epsilon_j)^2 \right)} \right] \\ &= \frac{8}{\delta\lambda^2} \left[1 - \sqrt{1 - \frac{\delta\lambda^2 t^2}{4} \max_{i \neq j} (\epsilon_i - \epsilon_j)^2} \right] \\ &\approx \frac{8}{\delta\lambda^2} \left[1 - 1 + \frac{\delta\lambda^2 t^2}{8} \max_{i \neq j} (\epsilon_i - \epsilon_j)^2 \right] \\ &= t^2 (\epsilon_{\max} - \epsilon_{\min})^2. \end{aligned} \quad (C1)$$

Finally, Eq. (77) follows from $\mathcal{H}_1 = \mathcal{H}_0^2$. So, $\epsilon_n = \varepsilon_n^2$, with ε_n eigenvalues of $\mathcal{H}_0 = L$, and $\varepsilon_{\min} = 0$ for simple graphs. \square

2. Cycle graph

Localized state According to the spectral decomposition in Table I, we consider the time-evolving localized state $|j(t)\rangle$ in Eq. (16). According to the definition of QFI in Eq. (58), we have to evaluate the following quantities

$$\langle \partial_\lambda j(t, \lambda) | \partial_\lambda j(t, \lambda) \rangle = 70t^2, \quad (C2)$$

$$|\langle j(t, \lambda) | \partial_\lambda j(t, \lambda) \rangle|^2 = 36t^2, \quad (C3)$$

since

$$\sum_{n=0}^{N-1} \left[2 \left(1 - \cos \left(\frac{2\pi j}{N} \right) \right) \right]^4 = 70N, \quad (C4)$$

$$\sum_{n=0}^{N-1} \left[2 \left(1 - \cos \left(\frac{2\pi j}{N} \right) \right) \right]^2 = 6N, \quad (C5)$$

from which follows the QFI in Eq. (64). Instead, the expression of the FI is tricky. Indeed, the expression of the probability in Eq. (17), or Eq. (18), is cumbersome and we can not find a more manageable form of the FI than its explicit definition in Eq. (59).

States maximizing the QFI In the cycle graph the ground state is unique, whereas the degeneracy of the highest energy level depends on the parity of N (see Table I). We define $E_\lambda = \varepsilon_{\max} + \lambda \varepsilon_{\max}^2$, where ε_{\max} is the highest energy eigenvalue of \mathcal{H}_0 (see Eq. (10) and Eq. (12) for even and odd N , respectively).

For even N , according to Eq. (78) the state maximizing the QFI is

$$|\psi_0(t)\rangle = \frac{1}{\sqrt{2N}} \sum_{k=0}^{N-1} [1 + (-1)^k e^{-iE_\lambda t}] |k\rangle, \quad (C6)$$

and the maximum QFI in Eq. (80) follows from the definition in Eq. (58). Then, the time-evolving probability distribution associated to a position measurement is

$$P_M(k, t|\lambda) = \frac{1}{N} [1 + (-1)^k \cos(E_\lambda t)] \quad (C7)$$

and has the following derivative

$$\partial_\lambda P_M(k, t|\lambda) = \frac{(-1)^{k+1}}{N} \varepsilon_{\max}^2 t \sin(E_\lambda t), \quad (C8)$$

being ε_{\max} defined in Eq. (10). Hence, observing that the dependence on the vertex is encoded only into an alternating sign, the FI is

$$\begin{aligned} \mathcal{F}_c(N, t, \lambda) &= \sum_{k=0}^{N/2-1} \left[\frac{(\partial_\lambda P_M(2k, t|\lambda))^2}{P_M(2k, t|\lambda)} + \frac{(\partial_\lambda P_M(2k+1, t|\lambda))^2}{P_M(2k+1, t|\lambda)} \right] \\ &= \frac{\varepsilon_{\max}^4 t^2 \sin^2(E_\lambda t)}{N^2} \sum_{k=0}^{N/2-1} \left[\frac{N}{1 + \cos(E_\lambda t)} + \frac{N}{1 - \cos(E_\lambda t)} \right] \\ &= \frac{\varepsilon_{\max}^4 t^2 \sin^2(E_\lambda t)}{N^2} \frac{N}{2} \frac{2N}{\sin^2(E_\lambda t)} = \varepsilon_{\max}^4 t^2 = \mathcal{F}_q(t). \end{aligned} \quad (C9)$$

In other words, the position measurement for the state maximizing the QFI in a cycle graph having an even number of vertices is optimal, since the corresponding FI equals the QFI.

For odd N , the situation is trickier: the state maximizing the QFI is not unique, because of the degeneracy

of the highest energy level. We may consider the two corresponding eigenstates according to Table I, which lead to the following states maximizing the QFI

$$|\varphi_0^\pm(t)\rangle = \frac{1}{\sqrt{2N}} \sum_{k=0}^{N-1} [1 + (-1)^k e^{\pm i\theta_k} e^{-iE_\lambda t}] |k\rangle, \quad (\text{C10})$$

where $\theta_k = \pi k/N$. On the other hand, as seen in Sec. II A, we may also consider the linear combinations of such eigenstates (see Eqs. (14)–(15)), which lead to the following states maximizing the QFI

$$|\psi_0^+(t)\rangle = \frac{1}{\sqrt{2N}} \sum_{k=0}^{N-1} [1 + \sqrt{2}(-1)^k \cos \theta_k e^{-iE_\lambda t}] |k\rangle, \quad (\text{C11})$$

$$|\psi_0^-(t)\rangle = \frac{1}{\sqrt{2N}} \sum_{k=0}^{N-1} [1 + \sqrt{2}(-1)^k \sin \theta_k e^{-iE_\lambda t}] |k\rangle. \quad (\text{C12})$$

Under the assumption of odd N , and according to the following results

$$\sum_{k=0}^{N-1} \cos^2 \theta_k = \sum_{k=0}^{N-1} \sin^2 \theta_k = \frac{N}{2}, \quad (\text{C13})$$

$$\sum_{k=0}^{N-1} (-1)^k e^{\pm i\theta_k} = \frac{1 + (-1)^N}{1 + e^{\pm i\theta_k}} \stackrel{\text{odd } N}{=} 0, \quad (\text{C14})$$

the maximum QFI in Eq. (80) follows from Eq. (58) and it does not depend on the choice of these states. Instead, we prove that the FI does depend on them.

Again, there is an alternating sign which depends on the vertex. In the following, we will split the sum over even and odd indices, and for odd N it reads as follows:

$$\sum_{k=0}^{N-1} a_k = \sum_{k=0}^{(N-1)/2} a_{2k} + \sum_{k=0}^{(N-1)/2-1} a_{2k+1}. \quad (\text{C15})$$

We first consider the states $|\varphi_0^\pm(t)\rangle$ in Eq. (C10). The time-evolving probability distribution associated to a position measurement is

$$P_M^\pm(k, t|\lambda) = \frac{1}{N} [1 + (-1)^k \cos(E_\lambda t \mp \theta_k)] \quad (\text{C16})$$

and has the following derivative

$$\partial_\lambda P_M^\pm(k, t|\lambda) = \frac{(-1)^{k+1}}{N} \varepsilon_{max}^2 t \sin(E_\lambda t \mp \theta_k), \quad (\text{C17})$$

being ε_{max} defined in Eq. (12). Hence the FI is

$$\begin{aligned} \mathcal{F}_c^\pm(|\varphi_0^\pm\rangle; N, t, \lambda) &= \\ &= \frac{\varepsilon_{max}^4 t^2}{N} \left[\sum_{k=0}^{(N-1)/2} \frac{\sin^2(E_\lambda t \mp \theta_{2k})}{1 + \cos(E_\lambda t \mp \theta_{2k})} \right. \\ &\quad \left. + \sum_{k=0}^{(N-1)/2-1} \frac{\sin^2(E_\lambda t \mp \theta_{2k+1})}{1 - \cos(E_\lambda t \mp \theta_{2k+1})} \right] \\ &= \frac{\varepsilon_{max}^4 t^2}{N} \left[\sum_{k=0}^{(N-1)/2} (1 - \cos(E_\lambda t \mp \theta_{2k})) \right. \\ &\quad \left. + \sum_{k=0}^{(N-1)/2-1} (1 + \cos(E_\lambda t \mp \theta_{2k+1})) \right] \\ &= \frac{\varepsilon_{max}^4 t^2}{N} \left[\frac{N-1}{2} + 1 + \frac{N-1}{2} - 1 + 1 \right] \\ &= \varepsilon_{max}^4 t^2 = \mathcal{F}_q(t, \lambda). \end{aligned} \quad (\text{C18})$$

Indeed, for odd N

$$\begin{aligned} &\sum_{k=0}^{(N-1)/2} \cos(E_\lambda t \mp \theta_{2k}) - \sum_{k=0}^{(N-1)/2-1} \cos(E_\lambda t \mp \theta_{2k+1}) \\ &= \sum_{k=0}^{N-1} (-1)^k \cos(E_\lambda t \mp \theta_k) = 0, \end{aligned} \quad (\text{C19})$$

since

$$\sum_{k=0}^{N-1} (-1)^k \cos \theta_k = \sum_{k=0}^{N-1} (-1)^k \sin \theta_k = 0. \quad (\text{C20})$$

Now, we focus on the state $|\psi_0^+(t)\rangle$ of Eq. (C11). The time-evolving probability distribution associated to a position measurement is

$$P_M^+(k, t|\lambda) = \frac{1}{2N} [1 + 2\sqrt{2}(-1)^k \cos \theta_k \cos(E_\lambda t) + 2 \cos^2 \theta_k] \quad (\text{C21})$$

and has the following derivative

$$\partial_\lambda P_M^+(k, t|\lambda) = \frac{\sqrt{2}(-1)^{k+1}}{N} \varepsilon_{max}^2 t \cos \theta_k \sin(E_\lambda t), \quad (\text{C22})$$

being ε_{max} defined in Eq. (12). Hence the FI is

$$\begin{aligned} \mathcal{F}_c^+(|\psi_0^+\rangle; N, t, \lambda) &= \frac{4\varepsilon_{max}^4 t^2 \sin^2(E_\lambda t)}{N} \\ &\times \left[\sum_{k=0}^{(N-1)/2} \frac{\cos^2 \theta_{2k}}{1 + 2\sqrt{2} \cos \theta_{2k} \cos(E_\lambda t) + 2 \cos^2 \theta_{2k}} \right. \\ &\quad \left. + \sum_{k=0}^{(N-1)/2-1} \frac{\cos^2 \theta_{2k+1}}{1 - 2\sqrt{2} \cos \theta_{2k+1} \cos(E_\lambda t) + 2 \cos^2 \theta_{2k+1}} \right]. \end{aligned} \quad (\text{C23})$$

Analogously for $|\psi_0^-(t)\rangle$ in Eq. (C12), we find

$$\begin{aligned} \mathcal{F}_c^-(|\psi_0^-\rangle; N, t, \lambda) &= \frac{4\varepsilon_{max}^4 t^2 \sin^2(E_\lambda t)}{N} \\ &\times \left[\sum_{k=0}^{(N-1)/2} \frac{\sin^2 \theta_{2k}}{1 + 2\sqrt{2} \sin \theta_{2k} \cos(E_\lambda t) + 2 \sin^2 \theta_{2k}} \right. \\ &\quad \left. + \sum_{k=0}^{(N-1)/2-1} \frac{\sin^2 \theta_{2k+1}}{1 - 2\sqrt{2} \sin \theta_{2k+1} \cos(E_\lambda t) + 2 \sin^2 \theta_{2k+1}} \right]. \end{aligned} \quad (C24)$$

Numerical results suggest that $\mathcal{F}_c^\pm(|\psi_0\rangle^\pm; N, t, \lambda) < \mathcal{F}_q(t, \lambda)$. Notice that $\mathcal{F}_c^\pm(|\psi_0\rangle^\pm; N, t, \lambda = -1/\varepsilon_{max}) = 0 \forall t$. Indeed, for such value of λ we have that $E_\lambda = 0$.

3. Complete graph

Localized state We consider the time-evolving localized state $|j(t)\rangle$ in Eq. (28). According to the definition of QFI in Eq. (58), we have to evaluate the following quantities

$$\langle \partial_\lambda j(t, \lambda) | \partial_\lambda j(t, \lambda) \rangle = t^2 N^3 (N-1), \quad (C25)$$

$$|\langle j(t, \lambda) | \partial_\lambda j(t, \lambda) \rangle|^2 = t^2 N^2 (1-N)^2, \quad (C26)$$

from which follows the QFI in Eq. (65). On the other hand, the probabilities of finding the walker in a certain position are provided in Eqs. (29)–(30) and their derivatives are

$$\partial_\lambda P_j(i \neq j, t|\lambda) = 2t \sin(2t\omega_N(\lambda)), \quad (C27)$$

$$\partial_\lambda P_j(j, t|\lambda) = -2(N-1)t \sin(2t\omega_N(\lambda)), \quad (C28)$$

being $\omega_N(\lambda)$ defined in Eq. (31). Then, according to Eq. (59), and since the starting vertex has probability (29), whereas the others $(N-1)$ have the same probability (30), we easily obtain the FI in Eq. (66).

States maximizing the QFI The complete graph has two energy levels: the ground state is unique, but the highest energy level is $(N-1)$ -degenerate (see Table II). The QFI does not depend on the choice of the eigenstate of the highest energy level, but the FI does. As an example, we consider two different states maximizing the QFI $|\psi_0^1\rangle$ and $|\psi_0^{N-1}\rangle$, i.e. the states in Eq. (81) for $l=1$ and $l=N-1$, respectively.

The first state is

$$|\psi_1^0(t)\rangle = \frac{1}{\sqrt{2}} \left[|e_0\rangle + \frac{1}{\sqrt{2}} e^{-2it\omega_N(\lambda)} (|0\rangle - |1\rangle) \right]. \quad (C29)$$

The time-evolving probability distribution associated to

a position measurement is

$$P_M^0(0, t|\lambda) = \frac{1}{4} + \frac{1}{2N} + \frac{\cos(2t\omega_N(\lambda))}{\sqrt{2N}}, \quad (C30)$$

$$P_M^0(1, t|\lambda) = \frac{1}{4} + \frac{1}{2N} - \frac{\cos(2t\omega_N(\lambda))}{\sqrt{2N}}, \quad (C31)$$

$$P_M^0(i, t|\lambda) = \frac{1}{2N}, \text{ with } 2 \leq i \leq N-1, \quad (C32)$$

and has the following derivatives

$$\partial_\lambda(P_M^0(0, t|\lambda)) = \frac{-tN^2}{\sqrt{2N}} \sin(2t\omega_N(\lambda)), \quad (C33)$$

$$\partial_\lambda(P_M^0(1, t|\lambda)) = \frac{tN^2}{\sqrt{2N}} \sin(2t\omega_N(\lambda)), \quad (C34)$$

$$\partial_\lambda(P_M^0(i, t|\lambda)) = 0, \text{ with } 2 \leq i \leq N-1. \quad (C35)$$

Then, being null the $(N-2)$ contributions from the vertices $2 \leq i \leq N-1$, only the probabilities associated to the vertices $|0\rangle$ and $|1\rangle$ contribute to the FI, which results in Eq. (85).

Similarly, the second state is

$$\begin{aligned} |\psi_0^{N-1}(t)\rangle &= \frac{1}{\sqrt{2}} \left\{ |e_0\rangle + \frac{1}{\sqrt{N^2-N}} e^{-2it\omega_N(\lambda)} [|0\rangle + \dots \right. \\ &\quad \left. + |N-2\rangle - (N-1)|N-1\rangle] \right\}. \end{aligned} \quad (C36)$$

The time-evolving probability distribution associated to a position measurement is

$$\begin{aligned} P_M^{N-1}(i \leq N-2, t|\lambda) &= \frac{1}{2(N-1)} + \frac{1}{N\sqrt{N-1}} \cos(2t\omega_N(\lambda)), \end{aligned} \quad (C37)$$

$$P_M^{N-1}(N-1, t|\lambda) = \frac{1}{2} - \frac{\sqrt{N-1}}{N} \cos(2t\omega_N(\lambda)), \quad (C38)$$

and has the following derivatives

$$\partial_\lambda P_M^{N-1}(i \leq N-2, t|\lambda) = \frac{-tN \sin(2t\omega_N(\lambda))}{\sqrt{N-1}}, \quad (C39)$$

$$\partial_\lambda P_M^{N-1}(N-1, t|\lambda) = tN\sqrt{N-1} \sin(2t\omega_N(\lambda)). \quad (C40)$$

Then, having $(N-1)$ equal contributions from the states $\{|i \leq N-2\rangle\}$ and a particular one from $|N-1\rangle$, the FI results in Eq. (86).

4. Star graph

Localized state We recall that considering the central vertex as the initial state provides the same results observed in the complete graph of the same size. Thus, we consider the time-evolving localized state $|j(t)\rangle$ in Eq. (43). According to the definition of QFI in Eq. (58), we have to evaluate the following quantities

$$\langle \partial_\lambda j(t, \lambda) | \partial_\lambda j(t, \lambda) \rangle = t^2 (N^2 + N + 2), \quad (C41)$$

$$|\langle j(t, \lambda) | \partial_\lambda j(t, \lambda) \rangle|^2 = 4t^2, \quad (C42)$$

from which follows the QFI in (68) .

According to Eq. (59), to evaluate the FI we also need the derivatives with respect to λ of the probability distribution in Eqs. (44)–(46):

$$\partial_\lambda P_1(0, t|\lambda) = 2t \sin(2\omega_N(\lambda)t), \quad (C43)$$

$$\begin{aligned} \partial_\lambda P_1(1, t|\lambda) = & -\frac{2t}{N(N-1)} \left[(N-2) \sin(2t\omega_1(\lambda)) \right. \\ & + (N-2)(N+1) \sin[2t(\omega_N(\lambda) - \omega_1(\lambda))] \\ & \left. + N \sin(2\omega_N(\lambda)t) \right], \quad (C44) \end{aligned}$$

$$\begin{aligned} \partial_\lambda P_1(i, t|\lambda) = & \frac{2t}{N(N-1)} \left[\sin(2t\omega_1(\lambda)) \right. \\ & + (N+1) \sin[2t(\omega_N(\lambda) - \omega_1(\lambda))] \\ & \left. - N \sin(2t\omega_N(\lambda)) \right], \quad (C45) \end{aligned}$$

with $2 \leq i \leq N-1$, from which the FI reads as

$$\begin{aligned} \mathcal{F}_c(N, t, \lambda) = & \frac{(\partial_\lambda P_1(0, t|\lambda))^2}{P_1(0, t|\lambda)} + \frac{(\partial_\lambda P_1(1, t|\lambda))^2}{P_1(1, t|\lambda)} \\ & + (N-2) \frac{(\partial_\lambda P_1(i, t|\lambda))^2}{P_1(i, t|\lambda)}. \quad (C46) \end{aligned}$$

States maximizing the QFI In the star graph the state maximizing the QFI, according to Eq. (89), is

$$|\psi_0(t)\rangle = \frac{1}{\sqrt{2}} (|e_0\rangle + e^{-2it\omega_N(\lambda)} |e_2\rangle), \quad (C47)$$

being both the ground and the highest energy levels not degenerate (see Table III). Then, the time-evolving probability distribution associated to a position measurement is

$$P_M(0, t|\lambda) = \frac{1}{2} + \frac{\sqrt{N-1}}{N} \cos(2t\omega_N(\lambda)), \quad (C48)$$

$$P_M(i \neq 0, t|\lambda) = \frac{1}{2(N-1)} - \frac{1}{N\sqrt{N-1}} \cos(2t\omega_N(\lambda)), \quad (C49)$$

and has the following derivatives

$$\partial_\lambda P_M(0, t|\lambda) = -tN\sqrt{N-1} \sin(2t\omega_N(\lambda)), \quad (C50)$$

$$\partial_\lambda P_M(i \neq 0, t|\lambda) = \frac{tN}{\sqrt{N-1}} \sin(2t\omega_N(\lambda)). \quad (C51)$$

Hence, the FI is

$$\begin{aligned} \mathcal{F}_c(N, t, \lambda) = & \frac{(\partial_\lambda P_M(0, t|\lambda))^2}{P_M(0, t|\lambda)} \\ & + (N-1) \frac{(\partial_\lambda P_M(i \neq 0, t|\lambda))^2}{P_M(i \neq 0, t|\lambda)}. \quad (C52) \end{aligned}$$

5. Maximum QFI states: the role of the phase factor in the superposition of energy eigenstates

So far we have studied the states maximizing the QFI without bothering to consider a different linear combination of the ground state and the highest energy state. According to the Parthasarathy's lemma 1, the two eigenstates defining the state in Eq. (75) are equally weighted. However, we may suppose the second one to have a phase factor, i.e

$$|\psi_0\rangle = \frac{1}{\sqrt{2}} (|e_0\rangle + e^{i\phi} |e_1\rangle). \quad (C53)$$

In this section, we study how the phase ϕ affects the FI and QFI of CTQWs on graphs. The states $|e_0\rangle$ and $|e_1\rangle$ denote the eigenstates of minimum and maximum energy eigenvalue, respectively, and we know that for simple graphs $|e_0\rangle = (1, \dots, 1)/\sqrt{N}$. Moreover, since the Laplacian matrix is real and symmetric, we can always deal with real eigenstates.

We already know that the QFI is (77) despite the presence of a phase shift. Indeed, by a straightforward calculation, we can easily verify that

$$\mathcal{F}_q(t) = t^2 [\partial_\lambda E_{max}^\lambda - \partial_\lambda E_{min}^\lambda]^2 = t^2 \varepsilon_{max}^4, \quad (C54)$$

where $E_{max}^\lambda = \varepsilon_{max(min)} + \lambda \varepsilon_{max(min)}^2$ and $\varepsilon_{min} = 0$ for simple graphs. To derive the FI for a position measurement we need the probability distribution, which is

$$\begin{aligned} P(i, t|\lambda) = & \frac{1}{\sqrt{N}} \cos(E_{max}^\lambda t - \phi) \langle i|e_1\rangle \\ & + \frac{1}{2} \left(\frac{1}{N} + \langle i|e_1\rangle^2 \right). \quad (C55) \end{aligned}$$

Indeed, dealing with real vectors, the resulting scalar products are real. The λ -derivative of this probability distribution is

$$\partial_\lambda P(i, t|\lambda) = -\frac{t\varepsilon_{max}^2}{\sqrt{N}} \sin(E_{max}^\lambda t - \phi) \langle i|e_1\rangle. \quad (C56)$$

Hence, the FI reads as follows:

$$\mathcal{F}_c(t|\lambda) = 2t^2 \varepsilon_{max}^4 \sin^2(E_{max}^\lambda t - \phi) \sum_{i=0}^{N-1} \frac{\langle i|e_1 \rangle^2}{N \langle i|e_1 \rangle^2 + 2\sqrt{N} \langle i|e_1 \rangle \cos(E_{max}^\lambda t - \phi) + 1} \quad (C57)$$

$$= 2t^2 \varepsilon_{max}^4 \sin^2(E_{max}^\lambda t - \phi) \sum_{i=0}^{N-1} \frac{\langle i|e_1 \rangle^2}{\left[\sqrt{N} \langle i|e_1 \rangle + \cos(E_{max}^\lambda t - \phi) \right]^2 + \sin^2(E_{max}^\lambda t - \phi)}. \quad (C58)$$

So, the phase is encoded as a phase shift in all the sine and cosine functions. However, this does not result in a

global time shift, because the quadratic term in t is not affected by ϕ .

-
- [1] E. Farhi and S. Gutmann, Phys. Rev. A **58**, 915 (1998).
 - [2] A. M. Childs, E. Farhi, and S. Gutmann, Quantum Inf. Process. **1**, 35 (2002).
 - [3] T. G. Wong, L. Tarrataca, and N. Nahimov, Quantum Inf. Process. **15**, 4029 (2016).
 - [4] S. Das and E. C. Vagenas, Physical review letters **101**, 221301 (2008).
 - [5] B. R. Rao, R. Srikanth, C. M. Chandrashekar, and S. Banerjee, Physical Review A **83** (2011), ISSN 1094-1622, URL <http://dx.doi.org/10.1103/PhysRevA.83.064302>.
 - [6] F. Caruso, New Journal of Physics **16**, 055015 (2014), ISSN 1367-2630, URL <http://dx.doi.org/10.1088/1367-2630/16/5/055015>.
 - [7] I. Siloi, C. Benedetti, E. Piccinini, J. Piilo, S. Maniscalco, M. G. A. Paris, and P. Bordon, Physical Review A **95** (2017), ISSN 2469-9934, URL <http://dx.doi.org/10.1103/PhysRevA.95.022106>.
 - [8] M. A. C. Rossi, C. Benedetti, M. Borrelli, S. Maniscalco, and M. G. A. Paris, Physical Review A **96** (2017), ISSN 2469-9934, URL <http://dx.doi.org/10.1103/PhysRevA.96.040301>.
 - [9] M. Cattaneo, M. A. C. Rossi, M. G. A. Paris, and S. Maniscalco, Physical Review A **98** (2018), ISSN 2469-9934, URL <http://dx.doi.org/10.1103/PhysRevA.98.052347>.
 - [10] M. A. C. Rossi, M. Cattaneo, M. G. A. Paris, and S. Maniscalco, Quantum Measurements and Quantum Metrology **5**, 4049 (2018), ISSN 2299-114X, URL <http://dx.doi.org/10.1515/qmetro-2018-0003>.
 - [11] L. De Santis, G. Coppola, C. Antn, N. Somaschi, C. Gmez, A. Lematre, I. Sagnes, L. Lanco, J. C. Lored, O. Krebs, et al., Physical Review A **99** (2019), ISSN 2469-9934, URL <http://dx.doi.org/10.1103/PhysRevA.99.022312>.
 - [12] A. A. Melnikov, L. E. Fedichkin, R. Lee, and A. Alodjants, Advanced Quantum Technologies **3**, 1900115 (2020), ISSN 2511-9044, URL <http://dx.doi.org/10.1002/quote.201900115>.
 - [13] A. M. Childs and J. Goldstone, Phys. Rev. A **70**, 022314 (2004).
 - [14] v. kendon, international journal of quantum information **04**, 791805 (2006), ISSN 1793-6918, URL <http://dx.doi.org/10.1142/s0219749906002195>.
 - [15] T. G. Wong and A. Ambainis, Physical Review A **92** (2015), ISSN 1094-1622, URL <http://dx.doi.org/10.1103/PhysRevA.92.022338>.
 - [16] T. G. Wong and D. A. Meyer, Physical Review A **93** (2016), ISSN 2469-9934, URL <http://dx.doi.org/10.1103/PhysRevA.93.062313>.
 - [17] P. Philipp, L. Tarrataca, and S. Boettcher, Physical Review A **93** (2016), ISSN 2469-9934, URL <http://dx.doi.org/10.1103/PhysRevA.93.032305>.
 - [18] M. Delvecchio, C. Groiseau, F. Petiziol, G. S. Summy, and S. Wimberger, Journal of Physics B: Atomic, Molecular and Optical Physics **53**, 065301 (2020), ISSN 1361-6455, URL <http://dx.doi.org/10.1088/1361-6455/ab63ad>.
 - [19] A. Ahmadi, R. Belk, C. Tamon, and C. Wendler, Quantum Information & Computation **3**, 611 (2003).
 - [20] N. Inui, K. Kasahara, Y. Konishi, and N. Konno, Fluctuation and Noise Letters **5**, L73 (2005).
 - [21] M. Jafarizadeh and S. Salimi, Annals of physics **322**, 1005 (2007).
 - [22] S. Salimi, Annals of Physics **324**, 1185 (2009).
 - [23] X.-P. Xu, Journal of Physics A: Mathematical and Theoretical **42**, 115205 (2009).
 - [24] A. M. Childs, Phys. Rev. Lett. **102** (2009).
 - [25] A. M. Childs and J. Goldstone, Phys. Rev. A **70** (2004).
 - [26] V. Kendon, Phil. Trans. R. Soc. A **364**, 3407 (2006).
 - [27] A. Ambainis, SIAM J. Comput. **37**, 210 (2007).
 - [28] E. Farhi, J. Goldstone, and S. Gutmann, Theory Comput. **4**, 169 (2008).
 - [29] J. K. Gamble, M. Friesen, D. Zhou, R. Joynt, and S. N. Coppersmith, Phys. Rev. A **81** (2010).
 - [30] O. Mülken and A. Blumen, Phys. Rep. **502**, 37 (2011).
 - [31] R. Alvir, S. Dever, B. Lovitz, J. Myer, C. Tamon, Y. Xu, and H. Zhan, J. Algebr. Comb **43**, 801 (2016).
 - [32] D. Tamascelli, S. Olivares, S. Rossotti, R. Osellame, and M. G. A. Paris, Sci. Rep **6**, 26054 (2016).
 - [33] M. Mohseni, P. Rebentrost, S. Lloyd, and A. Aspuru-Guzik, J. Chem. Phys. **129** (2008).
 - [34] S. Hoyer, M. Sarovar, and K. B. Whaley, New J. Phys **12**, 065041 (2010).
 - [35] P. M. Preiss, R. Ma, M. E. Tai, A. Lukin, M. Rispoli, P. Zupancic, Y. Lahini, R. Islam, and M. Greiner, Science **347**, 6227 (2015).
 - [36] A. Peruzzo, M. Lobino, J. C. F. Matthews, N. Matsuda, A. Politi, K. Poulios, X. Zhou, Y. Lahini, N. Ismail, K. Wörhoff, et al., Science **329**, 5998 (2010).

- [37] C. Moore and A. Russell, in *International Workshop on Randomization and Approximation Techniques in Computer Science* (Springer, 2002), pp. 164–178.
- [38] D. Aharonov, A. Ambainis, J. Kempe, and U. Vazirani, in *Proceedings of the thirty-third annual ACM symposium on Theory of computing* (ACM, 2001), pp. 50–59.
- [39] W. Adamczak, K. Andrew, P. Hernberg, and C. Tamon, ArXiv quant-ph/0308073 (2003).
- [40] D. J. Thouless, Physics Reports **13**, 93 (1974).
- [41] B. Kramer and A. MacKinnon, Reports on Progress in Physics **56**, 1469 (1993).
- [42] G.-L. Ingold, A. Wobst, C. Aulbach, and P. Hänggi, The European Physical Journal B-Condensed Matter and Complex Systems **30**, 175 (2002).
- [43] T. Baumgratz, M. Cramer, and M. B. Plenio, Phys. Rev. Lett. **113**, 140401 (2014).
- [44] R. M. Gray et al., Foundations and Trends® in Communications and Information Theory **2**, 155 (2006).
- [45] N. Konno, Physical Review E **72**, 026113 (2005).
- [46] T. Endo, S. Osano, K. Toyoshima, and Y. Hirayoshi, Journal of the Physical Society of Japan **78**, 064004 (2009).
- [47] A. Mirotin and E. Mirotin, Real Analysis Exchange **34**, 347 (2009).
- [48] M. G. A. Paris, International Journal of Quantum Information **7**, 125 (2009).
- [49] K. Newey and D. McFadden, *Large sample estimation and hypothesis* (Citeseer, 1994), chap. 36, pp. 2112–2245, theorem 3.3.
- [50] L. Seveso, M. A. C. Rossi, and M. G. A. Paris, Phys. Rev. A **95**, 012111 (2017), URL <https://link.aps.org/doi/10.1103/PhysRevA.95.012111>.
- [51] L. Seveso and M. G. A. Paris, Phys. Rev. A **98**, 032114 (2018), URL <https://link.aps.org/doi/10.1103/PhysRevA.98.032114>.
- [52] L. Seveso, F. Albarelli, M. G. Genoni, and M. G. A. Paris, Journal of Physics A: Mathematical and Theoretical **53**, 02LT01 (2019), URL <https://doi.org/10.1088/2F1751-8121%2F599b>.
- [53] K. Parthasarathy, in *Stochastics in finite and infinite dimensions* (Springer, 2001), pp. 361–377.
- [54] A. E. Brouwer and W. H. Haemers, *Spectra of graphs* (Springer Science & Business Media, 2011).
- [55] M. Fiedler, Czechoslovak mathematical journal **23**, 298 (1973).
- [56] B. Mohar, Y. Alavi, G. Chartrand, and O. Oellermann, Graph theory, combinatorics, and applications **2**, 12 (1991).
- [57] A. Marsden, University of Chicago, REU (2013).
- [58] M. Abramowitz and I. A. Stegun, *Handbook of mathematical functions: with formulas, graphs, and mathematical tables* (Dover Publications, Inc., New York, 1970).
- [59] L. Razzoli, M. G. Paris, and P. Bordone, Physical Review A **101**, 032336 (2020).
- [60] The further reason is that some numerical routines solving the eigenproblem for real symmetric matrices may return orthonormal eigenvectors with real components.
- [61] The linear combination leading to Eq. (15) introduces also an imaginary unit. However, this is a global phase factor, and, as such, we neglect it.
- [62] For even N the center of the cycle graph is not properly defined, i.e. is not unique. One can choose $|N/2 - 1\rangle \vee |N/2\rangle$.